

ACTA

Antti Järvenpää

MICROSTRUCTURES,
MECHANICAL STABILITY
AND STRENGTH OF LOW-
TEMPERATURE REVERSION-
TREATED AISI 301LN STAINLESS
STEEL UNDER MONOTONIC
AND DYNAMIC LOADING

UNIVERSITY OF OULU GRADUATE SCHOOL;
UNIVERSITY OF OULU,
FACULTY OF TECHNOLOGY



ACTA UNIVERSITATIS OULUENSIS
C Technica 695

ANTTI JÄRVENPÄÄ

**MICROSTRUCTURES, MECHANICAL
STABILITY AND STRENGTH OF
LOW-TEMPERATURE REVERSION-
TREATED AISI 301LN STAINLESS
STEEL UNDER MONOTONIC AND
DYNAMIC LOADING**

Academic dissertation to be presented with the assent of
the Doctoral Training Committee of Technology and
Natural Sciences of the University of Oulu for public
defence in the OP auditorium (L10), Linnanmaa, on 15
February 2019, at 12 noon

UNIVERSITY OF OULU, OULU 2019

Copyright © 2019
Acta Univ. Oul. C 695, 2019

Supervised by
Professor Jukka Kömi
Professor Pentti Karjalainen

Reviewed by
Professor Andrea Di Schino
Doctor Niilo Suutala

Opponents
Professor Horst Biermann
Doctor Niilo Suutala

ISBN 978-952-62-2169-4 (Paperback)
ISBN 978-952-62-2170-0 (PDF)

ISSN 0355-3213 (Printed)
ISSN 1796-2226 (Online)

Cover Design
Raimo Ahonen

JUVENES PRINT
TAMPERE 2019

Järvenpää, Antti, Microstructures, mechanical stability and strength of low-temperature reversion-treated AISI 301LN stainless steel under monotonic and dynamic loading.

University of Oulu Graduate School; University of Oulu, Faculty of Technology

Acta Univ. Oul. C 695, 2019

University of Oulu, P.O. Box 8000, FI-90014 University of Oulu, Finland

Abstract

Refining grain size is known to enhance mechanical properties also in austenitic stainless steels. To better understand the background of these properties, various reversion-treated structures were created in AISI 301LN (18Cr-7Ni-0.15N) steel and the microstructural features affecting flow behaviour and strength under monotonic and cyclic straining were investigated. Fully and partially reversed microstructures were produced using prior cold rolling thickness reductions in the range of 32–63% and both resistant and induction heating. Some selected reversed structures were also strengthening rolled to 20% reduction. The resultant microstructures were characterised using different research equipment and methods and their mechanical properties determined by microhardness, tensile and fatigue tests. The main interest was focused on the microstructural features of low-temperature reversed structures and the stability of austenite in them.

Effective grain refinement was achieved after 56–63% rolling reduction. Depending on the reduction and annealing conditions, the reversed structures consisted of various amounts of submicron- and medium-sized austenite grains and retained phases. All the reversed structures showed non-homogenous, often bimodal grain size distribution. It was demonstrated that the stability of austenite was much reduced after annealing at temperatures ≤ 850 °C, which was attributed to precipitation occurring at these low temperatures. Fine grain size itself promoted higher stability, but the coarsest retained austenite was stable due to its special orientation. Therefore, medium-sized grains of 3–10 μm , formed mainly from slightly deformed strain-induced martensite, appeared to be most unstable, the fraction being highest after the lowest reduction.

The yield and fatigue strengths of the low-temperature reversion-treated structures were significantly higher than those of commercial 301LN. Fatigue strength corresponded to that of a 20% cold-rolled sheet. Strength was highly enhanced even after the lowest cold rolling reduction of 32%, for the lower strength of the coarser reversed grain structure was balanced by the higher fractions of strong retained austenite and martensite phases.

Keywords: austenitic stainless steel, grain size refining, mechanical properties, mechanical stability, reversion treatment

Järvenpää, Antti, Matalan lämpötilan reversiorakenteiden mikrorakenteet, mekaaninen stabiilisuus ja lujuus monotonisessa ja sykklisessä kuormituksessa AISI 301LN teräksessä.

Oulun yliopiston tutkijakoulu; Oulun yliopisto, Teknillinen tiedekunta

Acta Univ. Oul. C 695, 2019

Oulun yliopisto, PL 8000, 90014 Oulun yliopisto

Tiivistelmä

Austeniitin raekoon hienontamisen tiedetään parantavan merkittävästi ruostumattomien terästen mekaanisia ominaisuuksia. Hienorakeisten reversiorakenteiden muokkauslujittumiseen ja lujuuteen vaikuttavien tekijöiden yksityiskohtaista tutkimista varten tuotettiin AISI 301LN (18Cr-7Ni-0.15N) teräkseen 32–63 % kylmävalssausreduktiota ja sen jälkeistä vastus- tai induktiokuumennusta käyttäen täysin sekä osittain reversoituneita mikrorakenteita. Lisäksi osa reversiorakenteista vielä lujitusvalssattiin 10–20 % reduktioon saakka. Mikrorakenteiden karakterisointiin käytettiin monipuolisesti eri tutkimuslaitteita ja menetelmiä sekä mekaanisten ominaisuuksien määrittämiseen mikrokovuus-, veto- ja väsytykskoikeita. Ensimmäisenä tarkoituksena oli tutkia yksityiskohtaisesti matalassa reversiolämpötilassa muodostuneita mikrorakenteita sekä hienorakeisen austeniitin stabiilisuutta monotonisessa ja sykklisessä kuormituksessa.

Reversiökäsitellyissä rakenteissa esiintyi vaihteleva määrä hienoja (raekoko alle 1 μm) ja keskisuuria (raekoko 3–10 μm) austeniittirakeita mahdollisten karkeiden jäännösfaasien lisäksi kylmämuokkausstilasta ja lämpökäsittely-parametreista riippuen. Suuri muokkausaste edesauttoi selvästi raerakenteen hienontumista, mutta kaikki rakenteet olivat raekokojakaumaltaan epähomogeenisia. Työssä demonstroititiin kuinka alle 900 °C:ssa hehkutetut reversiorakenteet ovat huomattavasti epästabiilimpia kuin korkeammassa syntyneet verokkirakenteet, minkä osoitettiin johtuvan krominitridien erkautumisesta. Raekoon hienontuminen itsessään suosii suurempaa stabiilisuutta, mutta karkeimmat muokkautuneet jäännösausteniittirakeet olivat stabiileja niiden orientaation takia. Täten keskisuuret rakeet olivat epästabiileimpia. Keskisuurien rakeiden osoitettiin syntyvän pääasiassa vähän muokkaantuneesta martensiitista, ja niitä esiintyi eniten 32% reduktiolla valssatuissa rakenteissa.

Matalassa lämpötilassa syntyneiden reversiorakenteiden lujuus oli merkittävästi korkeampi kuin kaupallisen teräksen. Väsymislujuus vastasi noin 20 % lujitettavalssattua tuotetta. Hehkutusta edeltänyt kylmämuokkausaste vaikutti vain vähän reversiorakenteiden lujuuteen, sillä vaikka pienin muokkausaste johti karkeimpaan keskimääräiseen raekokoon, siinä lujuutta lisäsivät kovat jäännösfaasit.

Asiasanat: austeniittinen ruostumaton teräs, mekaaniset ominaisuudet, raekoon hienontaminen, reversiökäsittely, stabiilisuus

Vilholle, Viljamille, Iinalle ja Miialle

Acknowledgements

This study was carried out in both the “Future Manufacturing Technologies” research group and the “Materials and Production Engineering” research unit of the Faculty of Technology at the University Oulu during the years 2009–2018. The research was funded by the Finnish Funding Agency for Technology and Innovation (Tekes) under the “Ultralujien levy materiaalien laseravusteinen muovattavuus” (ULLA) project, European structural funding under the “Tailored Small-Batch Steels with Enhanced Properties (RPST) project and Interreg Nord under the “Nordic Community for Fast Steel Heat Treatments” (NorFaST-HT) project. Personal grants awarded by Metallinjalostajien säätiö, Tauno Tönningin säätiö and Kerttu Saalasti säätiö are acknowledged with gratitude. Outokumpu Stainless Oy (Mr Timo Manninen) is acknowledged for providing the experimental material and valuable information on production conditions.

I am truly grateful for the continuous guidance and support received from many people during this study. I would like to acknowledge a few of them. Firstly, I thank my supervisors, Professor emeritus Pentti Karjalainen and Professor Jukka Kömi, for their support and guidance of my research. Special thanks and my sincere gratitude go especially to Pentti Karjalainen for the valuable time he has spent with me for innumerable discussions. I also thank Research Manager Kari Mäntyjärvi for his support of my work and funding applications, Seppo Järvenpää, Juha Uusitalo and Matias Jaskari for their assistance with the experimental research and Dr Jiří Man (IMP Brno, Czech) for valuable discussions. My thanks go to Professor Andrea Di Schino from the University of Perugia, Italy, and Dr Niilo Suutala (former director at Outokumpu Oyj) for their pre-examination of this thesis and their suggestions for improving the manuscript.

I would like to express my gratitude to my colleagues in the Future Manufacturing Technologies research group and the Materials and Production Engineering research unit for providing a fruitful and productive work environment and unconditional assistance in solving practical issues.

Finally, I want to thank my family and friends, my mom, dad and sisters and their families for their infinite support. I especially want to thank my dearest Miia, Viljami, Vilho and Iina for an endless number of things.

Antti Järvenpää

Symbols and abbreviations

| | |
|---------------------------|--|
| AGS | Average grain size |
| bcc | Body-centred cubic |
| CGA | Coarse-grained austenitic structure ($> 10 \mu\text{m}$) |
| CR | Cold rolling |
| DA | Deformed austenite (also in retained condition) |
| ε_{at} | Total strain amplitude [%] |
| DIM | Deformation-induced martensite |
| EBSD | Electron backscatter diffraction |
| fcc | Face-centred cubic |
| FSA | Fine-sized austenite ($< 3 \mu\text{m}$) |
| FGA | Fine-grained austenitic structure |
| GS | Grain size [μm] |
| HAGB | High angle grain boundary |
| IPF | Inverse pole figure |
| LAGB | Low angle grain boundary |
| MSA | Medium-sized austenite ($3\text{--}5 \mu\text{m}$) |
| ODF | Orientation distribution function |
| PRev | Partially reversed structure |
| RA | Reversed austenite |
| RD | Rolling direction |
| σ_{a} | Stress amplitude [MPa] |
| SHR | Strain hardening rate |
| SR | Shear-reversed austenite |
| TEI | Total elongation [%] |
| TEM | Transmission electron microscopy |
| TD | Transverse to the rolling direction |
| T_{p} | Annealing temperature [$^{\circ}\text{C}$] |
| t_{s} | Holding time [s] |
| UFGA | Submicron-sized austenitic structure |
| UEI | Uniform elongation [%] |
| UTS | Ultimate tensile strength [MPa] |
| UYP | Upper yield point [MPa] |
| wt.% | Weight fraction in per cents |
| XRD | X-ray diffraction |
| YS | Yield strength [MPa] |

List of original publications

This thesis is based on the following publications, which are referred to throughout the text by their Roman numerals:

- I Järvenpää, A., Jaskari, M., Man, J. & Karjalainen, L. P. (2017). Austenite stability in reversion-treated structures of a 301LN steel under tensile loading. *Materials Characterization*, 127, 12–26. <https://doi.org/10.1016/j.matchar.2017.01.040>
- II Järvenpää, A., Jaskari, M. & Karjalainen, L. P. (2014). Effect of grain size on fatigue behaviour of Type 301LN stainless steel. *International Journal of Fatigue*, 65, 93–98. <https://doi.org/10.1016/j.ijfatigue.2013.05.012>
- III Järvenpää, A., Jaskari, M., Man, J. & Karjalainen, L. P. (2017). Stability of grain-refined reversed structures in a 301LN austenitic stainless steel under cyclic loading. *Materials Science & Engineering A*, 703, 280–292. <https://doi.org/10.1016/j.msea.2017.07.033>
- IV Järvenpää, A., Jaskari, M., Juuti, T. & Karjalainen, L. P. (2017). Demonstrating the effect of precipitation on the mechanical stability of fine-grained austenite in reversion-treated 301LN stainless steel. *Metals* 7, 344. <https://doi.org/10.3390/met7090344>
- V Järvenpää, A., Jaskari, M. & Karjalainen, L. P. (2018). Reversed microstructures and tensile properties after various cold rolling reductions in AISI 301LN Steel. *Metals* 8, 109. <https://doi.org/10.3390/met8020109>
- VI Järvenpää, A., Jaskari, M. & Karjalainen, L. P. (2018). Properties of induction reversion-refined microstructures of AISI 301LN under monotonic, cyclic and rolling deformation. *Materials Science Forum*, 941, 601–607. <https://doi.org/10.4028/www.scientific.net/MSF.941.601>

Antti Järvenpää has been the main and corresponding author of all the publications. He has designed the research plans, carried out most of the experiments, except the Gleeble annealings for Papers I–V, XRD analysis for Papers I and III–V, TEM examinations for Paper IV and Thermocalc simulations for Paper IV, and written the drafts of all the manuscripts. Pentti Karjalainen has checked, commented and contributed to the writing of the manuscripts. Jirri Man has commented and improved Papers I and III and participated in developing the fatigue testing environment in the University of Oulu.

Paper I is a comprehensive study of reversed microstructures and austenite stability. The effect of different microstructural features, for example texture, grain size and its distribution and retained phases, were studied under monotonic straining.

Paper II is a tentative study of the fatigue behaviour of reversed structures under axial loading. The effect of different microstructural features on fatigue mechanisms, strength and cyclic stability were studied.

Paper III is a comprehensive study of the cyclic behaviour of reversed structures. Similarly as in Paper I, the effect of microstructural features on austenite stability was determined.

Paper IV demonstrates the effect of precipitation on austenite stability in low-temperature reversed structures. Stability measurements were carried out for subsequently annealed reversed structures. Precipitation kinetics was also predicted and precipitates were detected by transmission electron microscopy.

Paper V discusses and demonstrates the effect of prior cold rolling reduction on reversed microstructure, their features, behaviour and properties. Low rolling reductions were applied to study the effect of deformation especially on the formation of grains with different sizes.

Paper VI demonstrates industrial processing to manufacture and post-treat reversed structures. A pilot induction heat-treatment line was employed to produce reversed structures in sheets with larger dimensions. Some of the sheets were also subsequently cold-rolled for further strengthening. The fatigue strength of the reversed structures was studied in particular.

Table of contents

| | |
|---|-----------|
| Abstract | |
| Tiivistelmä | |
| Acknowledgements | 9 |
| Symbols and abbreviations | 11 |
| List of original publications | 13 |
| Table of contents | 15 |
| 1 Introduction | 17 |
| 1.1 Preface..... | 17 |
| 1.2 Metallurgical processes during reversion annealing | 19 |
| 1.3 Grain refinement by martensitic reversion..... | 20 |
| 1.4 Austenite stability | 22 |
| 1.4.1 Chemical composition and austenite stability | 23 |
| 1.4.2 The effect of grain size on austenite stability | 24 |
| 1.4.3 Additional features affecting austenite stability in low- temperature reversed structures..... | 25 |
| 1.5 Aims of the study | 26 |
| 2 Novel observations | 27 |
| 3 Experimental | 29 |
| 3.1 Cold-rolled test material AISI 301LN..... | 29 |
| 3.2 Research methods and equipment..... | 30 |
| 3.2.1 Annealing experiments..... | 30 |
| 3.2.2 Metallography | 31 |
| 3.2.3 Mechanical testing..... | 32 |
| 4 Results | 33 |
| 4.1 Microstructure of cold-rolled 301LN steel..... | 33 |
| 4.2 Microstructures of reversed structures | 35 |
| 4.2.1 Definitions of the microstructural features..... | 35 |
| 4.2.2 Phase structures | 38 |
| 4.2.3 Austenite grain sizes..... | 39 |
| 4.2.4 Texture of low-temperature reversed structures | 40 |
| 4.3 Mechanical stability of reversed structures | 42 |
| 4.3.1 Mechanical stability under monotonous deformation | 42 |
| 4.3.2 Cyclic and mechanical stability under fatigue loading..... | 44 |
| 4.3.3 Martensite nucleation under tensile straining..... | 46 |
| 4.3.4 Martensite nucleation under cyclic straining..... | 48 |

| | | |
|----------|---|-----------|
| 4.4 | Mechanical properties | 50 |
| 4.4.1 | Tensile properties of reversed structures | 50 |
| 4.4.2 | Cyclic strength of reversed structures..... | 51 |
| 4.4.3 | The effect of subsequent cold rolling deformation on monotonic and cyclic strength of reversed structures..... | 53 |
| 5 | Discussion | 55 |
| 5.1 | Low-temperature reversed structures | 55 |
| 5.1.1 | Grain size distributions affected by annealing temperature and cold rolling reduction..... | 55 |
| 5.1.2 | Formation of various austenite grain sizes in reversion | 57 |
| 5.2 | Stability of reversed structures | 59 |
| 5.2.1 | The role of grain size | 60 |
| 5.2.2 | The role of precipitation | 61 |
| 5.3 | Mechanical properties of reversed structures | 63 |
| 5.3.1 | Yield strength enhancement by refined grain size | 64 |
| 5.3.2 | Yield point and low strain hardening in grain-refined structures | 65 |
| 5.3.3 | Fatigue strength affected by microstructural features..... | 68 |
| 6 | Future studies | 73 |
| 7 | Summary and conclusions | 75 |
| | List of references | 77 |
| | Original publications | 87 |

1 Introduction

1.1 Preface

Austenitic stainless steels are the most used group of stainless steels, with a market share of about two-thirds. Their face-centred cubic crystal structure is achieved with sufficient alloying of nickel, manganese and nitrogen to stabilise the austenite phase. As a disadvantage, austenitic stainless steels are relatively expensive due to the high fraction of alloying elements. There are two sub-groups of austenitic stainless steels: a “leaner” 2XX series (Cr-Mn) and a “richer” 3XX (Cr-Ni) series. The latter has a higher fraction of nickel and is also more resistant to corrosion, but it is mechanically weaker due to a lower nitrogen content than in the 2XX series. (Charles et al., 2008).

In addition to various vessels, tanks, pipes and tubes in the process industry, austenitic stainless steels can also be used to improve safety and sustainability in automotive body structures, for instance in bus structures, tank trucks and trailers, etc. (Santacreu, Glez, Chinouilh & Fröhlich, 2006). High static strength is important in moving vehicles to save weight, but fatigue strength is also important.

Austenitic stainless steels possess a useful combination of mechanical properties, but their yield strength is generally low. Their excellent ductility and work hardening capability have typically been utilised to improve their strength by cold deformation (temper rolling) (Huang, Ye & Xu, 2012). Many Cr-Ni steels are metastable at room temperature, i.e. their austenite phase transforms to martensite under cold working. A disadvantage of this strengthening is the formation of anisotropy in mechanical properties (Taulavuori, Aspegren, Säynäjäkangas, Salmén & Karjalainen, 2004). For example, EUROCODE3 designing (EN 1993-1-1) determines the yield strength in longitudinal compression, the weakest load direction.

The grain size of commercial austenitic stainless steels is typically coarse, over 10 μm . Grain size refinement is an effective method for increasing the strength properties of metals and alloys (the well-known Hall-Petch relationship) and also their fatigue performance, especially in a high-cycle fatigue regime. Even though the impact of grain size on strength is not as high in austenitic stainless steels as in ferritic steels, refinement of grain size can provide significant improvement in yield strength. For example, ductile, ultrahigh strength ($> 700 \text{ MPa}$) has been achieved with a grain-refined austenitic structure in various 2XX and 3XX series alloys, as

reported in numerous papers during the last decades, e.g. (Di Schino, Barteri & Kenny, 2002; Di Schino, Salvatori & Kenny, 2002; Forouzan, Najafzadeh, Kermanpur, Hedayati & Surkialiabad, 2010; Jin, Jung & Lee, 2007; Kisko, Hamada, Karjalainen & Talonen, 2011; Maréchal, 2011; Misra et al., 2009; Somani, Juntunen, Karjalainen, Misra & Kyröläinen, 2009; Tomimura, Takaki, Tanimoto & Tokunaga, 1991; Tomimura, Takaki & Tokunaga, 1991).

The traditional hot rolling process or cold rolling and recrystallization annealing are not effective for grain size refinement of the austenite phase. However, reversion treatment, schematically illustrated in Fig. 1, can be an effective process. Reversion treatment to produce a fine-grained micron- or submicron-sized grain structure in austenitic stainless steels (experimental Cr-Ni alloys) was extensively examined in Japan by Tomimura, Takaki, Tanimoto & Tokunaga (1991) and Tomimura, Takaki & Tokunaga (1991) already in the 1980s, and in Italy by Di Schino, Barteri & Kenny (2002) and Di Schino, Salvatori & Kenny (2002) for 304- and 301-type Cr-Ni steels in the beginning of 2000, before recent extensive studies by Somani et al. (2009), Misra et al. (2009), Maréchal (2011) for 301LN-type steel, among many others. Furthermore, recent studies indicate that austenite stability is reduced in comparison with structures created at higher temperatures, which may provide new opportunities for improving static and dynamic mechanical properties (Baghbadorani et al., 2015; Iwamoto & Tsuta, 2000; Leal & Guimaraes, 1981; Misra, Zhang, Jia, Somani & Karjalainen, 2010; Nohara, Ono & Ohashi, 1977; Varma, Kalyanam, Murr, & Srinivas, 1994). As an example, Huang, Ye & Xu (2012) observed decreasing grain sizes with decreasing annealing temperatures down to 650 °C, and noted the validity of the Hall-Petch relationship.

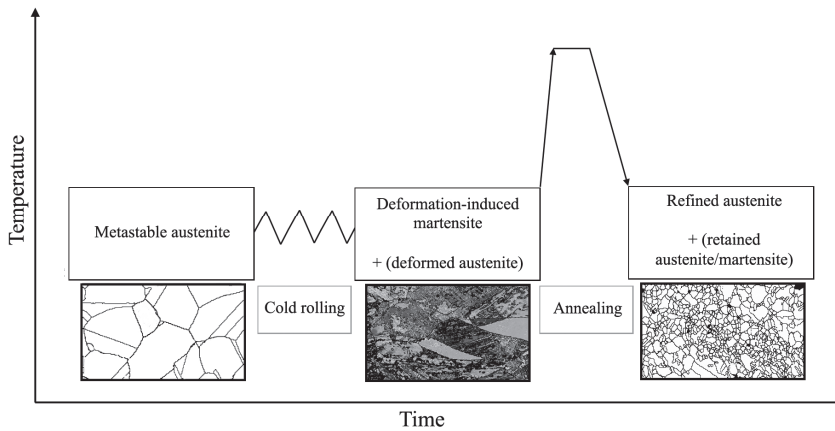


Fig. 1. Schematic illustration of reversion treatment.

1.2 Metallurgical processes during reversion annealing

In the present work, cold-worked metastable austenitic stainless steel was annealed for grain size refinement while different metallurgical processes took place. The stored energy of cold-deformed structures decreases during annealing, which can occur by two processes: recovery and recrystallization. Also, phase transformation can take place before, simultaneously with or following them. In austenitic stainless steel, the reversion of deformation-induced martensite to austenite is such a transformation.

During recovery, dislocation movement causes the removal of some dislocations and rearranges them to low-angle grain boundaries (LAGB), i.e. the amount of stored energy decreases and the properties change towards the values they had before deformation. During recovery, accumulated strain is relieved to some extent by microstructural and submicroscopic rearrangements, but the grains are not entirely strain-free. Recovery lowers the driving force for recrystallization, and for that reason may affect the nature and kinetics of recrystallization. Sometimes it is hard to define the division between recovery and recrystallization, because the recovery mechanisms play an important role in nucleating recrystallization. (Rollett, Rohrer & Humphreys, 2017)

In static recrystallization, new strain-free nuclei are formed, and growth of the nuclei exhausts the deformed structure (discontinuous recrystallization). Nucleation of new grains favours the vicinity of grain boundaries and slip planes.

It has also been suggested that nucleation occurs at cells formed in the recovery process (continuous recrystallization) and that the cells grow relatively quickly as long as the grain boundary angle remains low. The growth rate decreases until a high-angle boundary (HAGB) is formed between the cell nuclei and the surroundings. Once recrystallization is finished, grain growth occurs by diffusional movement of atoms across the grain boundaries. The driving force is the energy bound in the grain boundaries, and the growth rate depends on grain size. Finer grains have higher grain boundary energy, so they tend to grow quickly. (Cotterill & Mould, 1976; Rollett et al., 2017)

Martensitic reversion is a phase transformation in cold-deformed metastable austenitic stainless steel where deformation-induced martensite with a bcc-structure transforms back to fcc-austenite during annealing. Low-temperature reversion (≤ 800 °C) allows either work-hardened austenite or martensite to remain in the annealed structure to additionally enhance strength (Kisko et al., 2011). Reversion can occur by a diffusionless shear mechanism or a diffusion-controlled mechanism. Shear-reversed austenite inherits a strong substructure from cold-deformed martensite and recrystallizes later to fine-grained austenite (Somani et al., 2009; Tomimura, Takaki & Tokunaga, 1991). Diffusional reversion, on the other hand, is characterised by the nucleation and growth of randomly oriented equiaxed austenite grains at the cell or lath boundaries of the deformed martensite. It has been illustrated in the literature that martensite–austenite reversion by martensitic shear essentially depends on the chemical driving force (i.e., the chemical composition) and is independent of the amount of cold rolling reduction (Tomimura, Takaki & Tokunaga, 1991). For example, reversion in AISI 301 and 301LN occurs mainly by shear and diffusional reversion, respectively (Somani et al., 2009), although both mechanisms may be active during reversion, for instance in 301LN-type steel (Lee, Park, Lee, 2009).

1.3 Grain refinement by martensitic reversion

Numerous papers have shown that martensitic reversion (Fig. 1) is an effective method for refining the grain size (GS) of metastable austenitic stainless steels, including commercial grades such as AISI types 304, 301, 301LN, 201LN and 204Cu; e.g. (Di Schino, Barteri & Kenny, 2002; Di Schino, Salvatori & Kenny, 2002; Kisko et al., 2011; Somani et al., 2009). Micron and even submicron (sometimes called nano) GSs have been obtained during short annealing, while deformation-induced martensite (DIM) transforms into austenite (Tomimura,

Takaki, Tanimoto & Tokunaga, 1991; Tomimura, Takaki & Tokunaga, 1991; Somani et al., 2009). However, highly deformed cell-type martensite is a prerequisite source of a large number of nucleation sites for new austenite grains to attain this ultrafine GS of less than 1 μm (Misra, Nayak, Mali, Shah, Somani & Karjalainen, 2010; Misra, Zhang, Venkatasurya, Somani & Karjalainen, 2010; Takaki, Tomimura & Ueda, 1994; Tomimura, Takaki, Tanimoto & Tokunaga, 1991). A low degree of deformation of martensite tends to result in lath-type martensite, which transforms into austenite with morphological characteristics of the parent phase, but with a slightly coarser structure (Fargas, Zapata, Roa, Sapezanskaia & Mateo, 2015).

Complex processing routes are not desired in industrial practice, so interest should be focused on microstructures and properties achievable while using feasible lower cold rolling (CR) reductions, such as 50% or even less. Thickness reductions of 45–90% have been typically applied to metastable austenitic stainless steels (Kisko et al., 2011; Misra, Nayak, Venkatasurya, Ramuni, Somani & Karjalainen, 2010; Rajasekhara, Karjalainen, Kyröläinen & Ferreira, 2010; Somani et al., 2009; Tomimura, Takaki, Tanimoto & Tokunaga, 1991), and only scarce information is available on the effect of lower rolling reductions on grain refinement in the reversion process. Promisingly, in 301LN steel, even after CR reductions as low as 45%, submicron-sized austenite seemed to form during the reversion process (Somani et al., 2009). Fargas et al. (2015) showed that even very low reductions of 10–40% can reduce the average grain size (AGS) of 301LN steel by complete reversion, e.g. from 8.8 μm to 2.3 μm (40% prior rolling reduction), but the relative standard deviation was significantly increased, i.e. the GS distribution became broader while only a small fraction of grains was refined.

Different deformation states of martensite (GS of the reversed grains) and the presence of retained deformed austenite (DA) after low CR reductions tend to modify the structure, resulting in non-homogeneous GS distributions inherited from reversed DIM and recrystallized DA (Kisko, Hamada, Talonen, Porter & Karjalainen, 2016). Hence, the grain structure is often quite complex, especially that obtained at low annealing temperatures, T_p (≤ 800 ° C), which provide the highest strength with good ductility. Heterogeneous structures have been investigated and discussed by many authors, but only after heavy CR reductions (60% or above) (Kisko et al., 2016; Matsuoka, Iwasaki, Nakada, Tsuchiyama & Takaki, 2013; Ravi Kumar & Sharma, 2014). A bimodal grain structure could be beneficial for mechanical properties, while softer grains (GS larger than 1 μm) among hard submicron-sized grains enhance the ductility of the structure

(Eskandari Sabzi et al., 2016). Hence, due to these preliminary indications, the feasibility of low CR reductions calls for further studies to better understand their impact on the above-mentioned microstructural features and especially on the mechanical properties attained.

1.4 Austenite stability

Deformation-induced phase transformation is known to be beneficial in steels, enhancing the strain hardening rate and resulting in delayed local necking and thereby improving ductility and formability; e.g. (Tamura, 1982). This effect can be utilised in transformation-induced plasticity -aided carbon steels as well as metastable austenitic stainless steels. The stability of austenite against martensitic transformation depends on numerous factors such as temperature, chemical composition, crystallographic orientation, defect density, surrounding phases and GS (Iwamoto & Tsuta, 2010; Leal & Guimaraes, 1981; Lo, Shek & Lai, 2009; Misra, Zhang, Jia, Somani & Karjalainen, 2010; Nohara et al., 1977; Padilha, Plaut & Rios, 2003; Pereloma, Gazder & Timokhina, 2015; Takaki, Fukunaga, Syarif & Tsuchiyama, 2004; Varma et al., 1994).

It is well known that DIM formation can also take place in metastable austenitic stainless steels during cyclic loading, e.g. (Botshekan, Degallaix & Desplanques, 1997; Böhner et al., 2012; Di Schino & Kenny, 2003; Hahnenberger, Smaga & Eifler, 2014; Hennessy, Steckel & Altstetter, 1976; Krupp, West & Christ, 2008; Muller-Bollenhagen, Zimmermann & Christ, 2010; Smaga, Walther & Eifler, 2008; Topic, Tait & Allens, 2007), where it can have a considerable effect on both cyclic stress-strain behaviour and fatigue life (Böhner et al., 2012; Di Schino & Kenny, 2003; Krupp et al., 2008; Muller-Bollenhagen et al., 2010; Smaga et al., 2008; Topic et al., 2007). Susceptibility to DIM transformation under cyclic loading also strongly depends on, e.g. temperature, strain rate and even slight variations in chemical composition; e.g. (Das, Tarafder & Chakraborti, 2011; Man et al., 2018; Muller-Bollenhagen et al., 2010). However, the impact of GS and its distribution, retained phases and chemical inhomogeneity on austenite stability under both monotonic and cyclic loading has not been described to explain the behaviour of complex reversed structures.

1.4.1 Chemical composition and austenite stability

The chemical composition of steel affects phase stability, and many austenitic Cr-Ni and Cr-Mn stainless steel grades are metastable, i.e. austenite tends to transform to martensite under deformation. Empirical regression equations have been proposed to estimate the martensite fraction, including the influence of chemical composition (Angel, 1954; Nohara et al., 1977), as reviewed by Padilha et al. (2003) and Lo et al. (2009). A quantitative guideline regarding the effect of steel composition on strain-induced martensite formation is the M_{d30} temperature, where 50% strain-induced martensite is present after 30% tensile deformation. A commonly used Equation for M_{d30} is given by Nohara et al. (1977), Equation (1):

$$M_{d30} (\text{°C}) = 552 - 462(C+N) - 9.2Si - 8.1Mn - 13.7Cr - 29(Ni+Cu) - 18.5Mo - 68Nb - 1.42(GS-8) \quad (1)$$

where the elements are in wt.% and GS is the ASTM grain size. However, in practical multipass CR, the martensite fraction is highly dependent on pass reduction, as large passes result in much-reduced fractions, obviously due to adiabatic heating occurring in CR (Karjalainen, Taulavuori, Sellman & Kyröläinen, 2008).

From the above Equation it is seen that nitrogen is a strong austenite stabiliser, its effectiveness being equal to (Angel, 1954; Nohara et al., 1977) or stronger (Lee, Oh & Kim, 2008) than that of carbon. It is well known that the stability of austenite in nitrogen-alloyed stainless steels will be reduced if nitrogen precipitates out of the solid solution (Lo et al., 2009; Padilha et al., 2003; Simmons, Covino, Hawk & Dunning, 1996). In high-nitrogen steels, precipitation of Cr_2N has been found to occur over a temperature regime of 600–1050 °C, sometimes starting at grain boundaries, followed by discontinuous precipitation (cellular phase formation), and finally taking place intragranularly within the matrix (Lo et al., 2009). Precipitation kinetics vary highly depending on alloy composition and temperature, being primarily controlled by Cr diffusion; e.g., (Machado, Carvalho & Padilha, 2015; Shi, Wang, Cui & Liu, 2008; Simmons, 1996; Simmons, Covino, Hawk & Dunning, 1996). In certain alloys, the fastest kinetics can exist at 800 °C (Shi et al., 2008). It can be noted that 800°C is the common temperature used for reversion treatments. Rajasekhara, Ferreira, Karjalainen & Kyröläinen (2007) and Rajasekhara et al. (2010) observed the precipitation of CrN during reversion treatments in 301LN steel in transmission electron microscopy examinations. Therefore, the question

arises: what is the role of precipitation in austenite stability in low-temperature reversed structures? The answer was sought and revealed in this work.

1.4.2 The effect of grain size on austenite stability

Grain size in reversion-treated structures is much finer than in conventional austenitic stainless steels, and the potential impact of fine GS on austenite stability, and consequently on mechanical properties, is an important issue. In the past, several researchers have clarified experimentally the dependence of austenite stability and deformation behaviour on GS in austenitic stainless steels, see e.g. (Iwamoto & Tsuta, 2010; Leal et al., 1981; Misra, Zhang, Jia, Somani & Karjalainen, 2010; Nohara et al., 1977; Varma et al., 1994). Nohara et al. (1977) reported that the volume fraction of DIM under a given strain decreases linearly with decreasing GS. The higher strength of finer grains is suggested to be a reason for increased stability (Jin et al., 2007), although it is also argued that stability is based on dilatation energy, the physical energy associated with austenite-to-martensitic transformation (Misra, Wan, Challa, Somani & Murr, 2015; Takaki et al., 1994). Furthermore, effective stacking fault energy increases with decreasing GS (Jun & Choi, 1998; Lee & Choi, 2000), which can be assumed to be a factor that increases the stability of fine-sized austenite grains.

The trend of higher stability with decreasing GS is well established in “conventional” coarse-grained austenitic stainless steels where the grains are typically larger than about 10 μm , although even then, at least a couple of opposite results exist (De et al., 2006; Shrinivas, Varma & Murr, 1995). Further, Matsuoka et al. (2013) stated that DIM formation is independent of GS in tensile deformation, for tensile strain aids the formation of certain single martensite variants inside fine grains, so that dilatation energy is not a restricting factor. However, recently when ultrafine-grained austenitic (UFGA) steels have been processed, there have been observations of a more complicated dependence, suggesting that in the case of submicron GSs, austenite stability again decreases significantly.

The inverse dependence on GS of the UFGA structure in reversion-treated stainless steels was recorded the first time in tensile tests of 301LN steel by Somani et al. (2009). Hamada, Karjalainen, Venkata Surya & Misra (2011) also found that martensite tends to form earlier in the UFGA structure ($\text{GS} \approx 0.75 \mu\text{m}$) than in the coarse-grained austenite (CGA) structure ($\text{GS} \approx 20 \mu\text{m}$). Maréchal (2011) documented the same trend in similar 301LN steel, observing the lowest DIM fractions with an average austenite GS of 0.9 μm , whereas higher fractions were

seen with both increasing and decreasing GSs. Consistently, Kisko, Misra, Talonen & Karjalainen (2013) reported that in 204Cu-type Cr-Mn low-Ni austenitic stainless steel, the highest austenite stability was in the fine-grained austenite structure with a GS range of 1–2 μm . Behjati, Kermanpur, Najafizadeh & Samaei Baghbadorani, (2014) noticed that in 17.5Cr-11.5Mn-0.25N-0.05C (all concentrations are hereafter in wt.%) steel with an AGS of 0.24 μm , about 35% DIM was formed under tensile straining, whereas only 10% DIM was formed in an alloy with a 6 μm GS.

Nucleation of DIM at grain boundaries has been suggested as the reason for reduced stability in UFGA structures (Kisko et al., 2013; Maréchal, 2011). Recently, Wang, Tasan, Ponge, Kostka & Raabe (2014) recorded the lower stability of finer grains in maraging steel. They suggested that mechanical twinning, being more pronounced in large grains, inhibits martensite formation in large grains. However, as an opposing trend, Misra et al. (Misra, Zhang, Jia, Somani & Karjalainen, 2010; Misra, Zhang, Jia, Venkat Surya, Somani & Karjalainen, 2011; Misra, Wan et al., 2015, Misra, Challa, Venkatsurya, Shen, Somani & Karjalainen, 2015) did not find martensite formation, but twinning in ultrafine-grained 301LN steel, deformed by nano-indentation or tensile straining. The same finding has recently been reported also for 16Cr-10Ni steel (Challa, Misra, Somani & Wang, 2016).

1.4.3 Additional features affecting austenite stability in low-temperature reversed structures

Reversed structures are often complex, for in addition to refined grains they also contain coarser grains of DA and/or DIM, since in most cases all austenite has not transformed to martensite during the CR stage. For instance, in experiments by Kisko et al. (2013, 2016), 40% DA was present in the UFGA structure after CR was applied. Recovered DA is typically as hard as the UFGA structure (Kisko et al., 2011). Maréchal (2011) investigated a UFGA structure containing about 30% DA as well as some larger grains after annealing at 800 °C, which structure showed the lowest austenite stability in his tests. The presence of these additional microstructural features has not, however, been taken into account in previous investigations when explaining austenite stability.

1.5 Aims of the study

The aim of this study was to investigate in more detail than earlier the complex features of reversion-treated structures created at low T_p s in 301LN-type steel. Further, the effect of these complex microstructural features on austenite stability and tensile and fatigue properties were studied and the reason for the low stability of low-temperature reversed fine-grained structures was investigated. Even strengthening of the reversed structures by subsequent CR was tried. A practical aim was to optimise the prior CR operation for practical processing. The objective of this work can be divided into the following tasks:

- To characterise the complex features of non-homogenous reversed microstructures, affected by prior CR reduction and annealing conditions
- To better understand the features affecting the monotonic and cyclic behaviour and properties of reversed structures
- To clarify the different factors affecting austenite stability in complex reversed microstructures. Especially the effect of GS needed clarification
- To study the effect of subsequent CR deformation on the behaviour and mechanical properties of low-temperature reversed structures.

2 Novel observations

To the best knowledge of the author, the following findings are original to this work:

- Low-temperature reversed microstructures formed in 301LN steel are complex, but now described in much more detail than previously.
- Medium-sized austenite (MSA) grains with a GS between 3 and 10 μm are shown to form mainly from slightly deformed strain-induced martensite. The origin, formation mechanisms and significant role of these grains during subsequent deformation are explained.
- The stability of reversed structures under dynamic and rolling loading varies similarly as under tensile loading.
- The high susceptibility of low-temperature reversed austenite to transform to martensite during deformation is not the result of the low stability of submicron grains, as claimed earlier.
- Low stability is partly the result of a high fraction of MSA grains, but is primarily caused by rapid chromium nitride precipitation below 850 °C.
- Strain-induced martensite formation under dynamic loading does not vary significantly between reversed structures, but its impact on cyclic hardening is different in grain-refined structures than in coarse-grained counterparts.
- CR reductions as low as 32% provide equivalent tensile properties as 63% reduction, although grain refinement remains much fainter.
- The fatigue strength of low-temperature reversed structures is highly enhanced compared with that of commercial sheets.
- Strengthening of reversed structures by subsequent CR is not efficient due to the low work-hardening of refined austenite grains. Neither tensile properties nor fatigue strength were improved significantly.

3 Experimental

3.1 Cold-rolled test material AISI 301LN

All experimental tests were carried out using commercial austenitic 18Cr-7Ni-0.15N (in wt.%) AISI 301LN-type stainless steel. Two sheets from different batches of industrial charges were received from Outokumpu Stainless Oy (Tornio, Finland). A 5.5 mm sheet (coded Set 1 in Paper I) was skin pass-rolled (C850 grade) and an 8 mm sheet (coded Set 2 in Paper I) was only hot-rolled and annealed. The chemical compositions of both sheets were very close to each other, as shown in Table 1. The corresponding M_{d30} temperatures according to the Nohara formula (Nohara et al., 1977) (Equation 1) were 16 °C and 23 °C for Set 1 and Set 2, respectively, indicating a slight difference in austenite stability (the difference is highlighted in Paper I). Both sheets were cold-rolled to ~63% thickness reduction (3.00 mm final thickness), but the Set 2 sheet was also cold-rolled to 32% (5.45 mm) and 56% (3.45 mm) reductions in a laboratory rolling mill in Tornio. These sheets were coded as 32CR, 56CR and 63CR, based on the rolling reduction. Some of the 56CR sheets were cold-rolled also subsequent to reversion annealing. The temperature during CR was kept below 50 °C by cooling the sheets in a subzero environment between passes. The reduction in each pass was below 5% and it decreased as the DIM fraction increased, so that the final passes caused approximately 1% reduction.

The Set 1 sheet was only used in Papers I and II, whereas the Set 2 sheet was the material in the Papers III–VI. Excluding the slight difference in austenite stability between the sheets of Set 1 and Set 2, the relative order of stability of the different structures and the same conclusions are valid for both sheets, so for simplicity, this thesis does not present separate results for these sets; both sets are referred to as “301LN” from here on.

Table 1. Chemical compositions (wt.%) of the AISI 301LN batches (Set 1 and Set 2) investigated. (Modified from Paper I).

| Steel | C | Si | Mn | Cr | Ni | Cu | N | Mo | P | Fe | Md30 |
|-------|-------|------|------|------|-----|------|-------|------|-------|------|------|
| Set 1 | 0.025 | 0.42 | 1.23 | 17.8 | 6.5 | 0.17 | 0.165 | 0.08 | 0.025 | bal. | 16 |
| Set 2 | 0.025 | 0.53 | 1.25 | 17.5 | 6.5 | 0.20 | 0.150 | 0.09 | 0.024 | bal. | 23 |

3.2 Research methods and equipment

3.2.1 Annealing experiments

The cold-rolled specimens were annealed at the University of Oulu with a Gleeble 3800 thermo-mechanical simulator that uses resistance heating (Papers I–V). The heating rate in the Gleeble experiments was 200 °C/s and the cooling rate was 25–35 °C/s depending on the specimen's thickness (25 °C/s with 32CR and 35 °C/s with 63CR sheets). The specimens were annealed at 750, 800, 900 and 1050 °C for 0.1, 1, 1, and 100–200 s, respectively. The duration of 0.1 s was achieved by setting the holding time (t_s) to zero. To understand the microstructural evolution during the low-temperature reversion process more deeply, additional structures were created at 700 °C (0.1–1.0 s) for the 32CR sheet.

In addition to Gleeble annealing, cold-rolled 32CR and 56CR sheets (~200 x 750 mm, width x length) were annealed at the ELME centre in Nivala on an induction pilot line equipped with a 600 kW longitudinal induction coil (frequency ~140 kHz) (Paper VI). Depending on the sheet thickness, the heating rate varied in the range of 110–220 °C/s below the Curie point and in the range of 22–30 °C/s above it. Induction annealing was followed by slow free cooling (1–3 °C/s).

The different reversed structures and their processing routes are listed in Table 2. This work focuses particularly on the partially reversed structures created by resistant heating at relatively low T_p s of 700–750 °C for 0.1 s (32CR and 63CR sheets; Papers I–V) or by induction at 690 °C (32CR and 56CR sheets; Paper VI). The codes of the specimens are based on CR reduction, T_p s and t_s . A commercial sheet (Com-301LN) used for reference was a hot-rolled sheet from the company.

Table 2. List of the different structures and their processing parameters presented in this work.

| Code | State | Publication | Heating type | CR [%] | T _p [°C] | t _s [s] |
|---------------|---------------------|----------------------|--------------|--------|---------------------|--------------------|
| 32CR-700-0.1 | Partially reversed | Paper V | Resistance | 32 | 700 | 0.1 |
| 63CR-700-0.1 | Partially reversed | Paper V | Resistance | 63 | 700 | 0.1 |
| 32CR-750-0.1 | Partially reversed | Paper V | Resistance | 32 | 750 | 0.1 |
| 63CR-750-0.1 | Partially reversed | Papers I, II, IV, V | Resistance | 63 | 750 | 0.1 |
| 32CR-690-60 | Partially reversed | Paper VI | Induction | 32 | 690 | ~70 |
| 56CR-690-60 | Partially reversed | Paper VI | Induction | 56 | 690 | ~60 |
| 63CR-800-1 | Completely reversed | Papers I–III, V | Resistance | 63 | 800 | 1 |
| 32CR-900-1 | Completely reversed | Paper V | Resistance | 32 | 900 | 1 |
| 63CR-900-1 | Completely reversed | Papers I, III, IV, V | Resistance | 63 | 900 | 1 |
| 63CR-1050-200 | Recrystallized | Papers I, II, V | Resistance | 63 | 1050 | 200 |
| Com-301LN | Recrystallized | Paper VI | Hot rolling | - | - | - |

3.2.2 Metallography

An optical laser scanning microscope (Keyence VK-X200) and a field emission scanning electron microscope (Zeiss Ultra Plus FEG-SEM) together with an electron backscatter diffraction (EBSD) unit (HKL EBSD detector) were used for the extensive microstructural examinations. Both surface and cross-sectional (the RD normal to the sheet surface plane) views were taken, the latter close to the sheet surface, about 0.1–0.2 mm below the edge.

A transmission electron microscope (TEM) (Jeol JEM-2200FS STEM) at 200 kV with an EDS unit and nanobeam diffraction was briefly used to identify Cr_xN precipitation in the reversed structures.

An X-ray diffractometer (XRD) (Rigagu Smartlab) was applied to determine the bulk crystallographic textures of the specimen surface layers after various treatments. The martensite fraction in the cold-rolled condition was determined using the same equipment with Co K α radiation (40 kV and 40 mA) and Rietveld WPPF (whole powder pattern fitting) analysis.

Ferromagnetic α' -martensite fractions were determined by magnetic measurements using a Feritscope® (Helmut Fisher FMP 30) instrument during tensile straining and cyclic loading. The readings of the Feritscope were multiplied by a correction factor of 1.7 according to Talonen, Aspegren & Hänninen (2004) and Beese & Mohr (2011). Except in Paper V, martensite evolution during tensile straining was measured by interrupting the tensile straining without unloading the

specimen and by interrupting cycling in dynamic tests (Paper III). DIM fractions were measured on the rolled surfaces for monotonic straining. In cyclic tests, magnetic measurements were taken on one edge (cross-section) of the polished specimens. Different measurement techniques had to be applied because the thinnest specimens (63CR) were fatigue tested using a buckling holder, and the surfaces were covered by the holder.

3.2.3 Mechanical testing

The evolution of DIM and the mechanical properties achieved were determined by tensile testing (a Zwick 100 machine) and cyclic loading (an MTS-810 machine). To avoid any adiabatic heating during tensile testing, a low true strain rate (0.0005 s^{-1}) was adopted. The strain rate during cyclic straining was relatively high and varied depending on the strain amplitude: $4.8 \times 10^{-2} \text{ s}^{-1}$ (total strain amplitude, $\epsilon_{\text{at}} \leq 0.2\%$), $7.2 \times 10^{-2} \text{ s}^{-1}$ ($\epsilon_{\text{at}} = 0.3\%$), $6.4 \times 10^{-2} \text{ s}^{-1}$ ($\epsilon_{\text{at}} = 0.4\%$) and $2.4 \times 10^{-2} \text{ s}^{-1}$ ($\epsilon_{\text{at}} = 0.6\%$). External air cooling by blown air was used during cyclic loading to restrict adiabatic heating.

The shape and dimensions of the specimens are shown in Fig. 1. In tensile testing, the width of the specimen gauge section was 6 mm (in Papers IV–VI) and 10 mm (in Papers I, II and IV) and the length was 25 mm. The thickness varied depending on the degree of CR reduction. In Paper VI, specimen geometry based on the EN-10002 standard was used (the width of the gauge section was 12.5 mm and length, 50 mm). For all the fatigue specimens the width of the gauge section was 10 mm and the length, 12.5 mm. To prevent stress concentration, the edges were rounded by grinding to approximately a 1 mm radius. Nominal stress values were calculated for mechanical analysis.

The microhardness (a load of 0.25 N) of austenite with different GSs and DIM was measured using a CSM MHT-Z-AE tester with a Vickers indenter. The measurements were repeated ten times at each location to obtain an average value.

4 Results

4.1 Microstructure of cold-rolled 301LN steel

For the martensitic reversion process, heavy CR reduction is desired to obtain deformed DIM. In Fig. 2 the DIM fractions formed during CR are plotted as a function of CR thickness reduction, determined by a Feritscope (for reductions $\leq 20\%$) and XRD (reductions $\geq 32\%$) (Paper V). It is seen that in the studied 301LN steel, the austenite phase transforms gradually to DIM, and to achieve a fully martensitic structure, CR reductions over 63% are required. This is in qualitative agreement with previous observations, the exact DIM values depending on the rolling parameters; e.g., (Fargas et al., 2015; Rajasekhara et al., 2010; Somani et al., 2009).

It can be mentioned that the DIM fractions measured on the cross-sections of the specimens tended to be slightly higher than those measured on the sheet surface. Segregation present in the centreline region and its effect on DIM formation during CR or tensile and cyclic straining were demonstrated in Papers I and III, but also in separate publications (Man et al., 2018). The DIM fractions in Fig. 2 present average values from the cross-sections, thereby including the centreline and the area close to the surface regions.

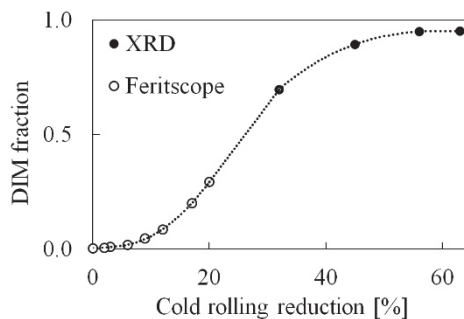


Fig. 2. Evolution of DIM in Com-301LN under the cold rolling conditions used in the study. (Reprinted by permission from Paper V © 2018 MDPI).

The phase fractions after the CR reductions are listed in Table 3. It is seen that the DIM fractions in the sheets used for the reversion annealing experiments were 70%, 95% and 96% for 32CR, 56CR and 63CR, respectively, so the retained DA fractions were correspondingly 30%, 5% and 4% (Papers I–VI).

Table 3. Phase fractions and estimated deformation states of the DIM phase. High deformation > 10% reduction.

| Sheet | Phase fractions | | | |
|-------|-----------------|-----------------|------------------|----|
| | DIM | | | DA |
| | Total | Low deformation | High deformation | - |
| 32CR | 70 | 30 | 40 | 30 |
| 56CR | 95 | 8 | 87 | 5 |
| 63CR | 96 | 7 | 89 | 4 |

Because of the gradual transformation of DIM, the local amount of deformation of DIM varies depending on which stage it has been formed in. The degree of deformation, in turn, affects the structure of DIM – lath- or cell-type – which plays a significant role in the evolution of the microstructure during reversion annealing (Section 4.2). The deformation structures of DIM and DA have been examined in detail by TEM in numerous publications, e.g. (Rajasekhara et al., 2007, 2010), so it was concluded that further examinations would hardly provide much new information and were not done in this study. From Fig. 2 it is possible to estimate qualitatively the degree of deformation of DIM encountered at different stages of CR, affecting the number of nucleating sites in the reversion. We can define, for instance, that reduction up to 10% is low. Then it can be seen that there is about 30%, 8% and 7% slightly-deformed DIM in the 32CR, 56CR and 63CR structures, respectively (Table 3).

Examples of the cold-rolled 32CR and 56CR microstructures are shown in Fig. 3. The 32CR structure consists of large DA grains (grey grains in Fig. 3a) with some substructure (white lines) in addition to band-like fragments of partially transformed DIM grains. The DIM (blue colour) appears as either banded or block-like grains. After 56% (Fig. 3c) and 63% rolling reductions, the structures were almost completely martensitic and the few remaining DA grains were smaller in size due to fragmentation.

The effect of CR reduction on the orientation of the DA grains is clearly seen by comparing the inverse pole figure (IPF) maps in Figs. 3b and 3d. Both the greenish and bluish colours were present in the 32CR structure (Fig. 3b), corresponding to the Brass $\{110\}\langle 211\rangle$ and Goss $\{110\}\langle 100\rangle$ texture components, respectively, but only greenish DA grains were detected in the 56CR (Fig. 3d) and 63CR structures. The deformation is seen as numerous LAGBs (white lines), while HAGBs are coloured black.

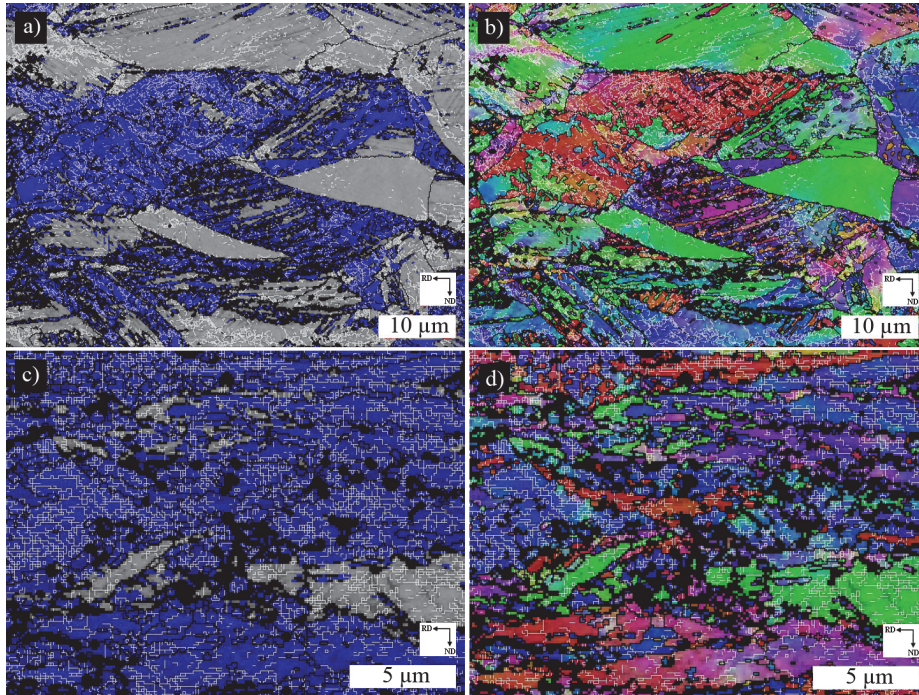


Fig. 3. Cold-rolled 32CR (a,b) and 56CR (c,d) structures in EBSD grain boundary maps overlapped with phase (left images) and IPF maps (right images). Grains with different colours: DIM = blue, DA = grey and unindexed pixels = black. White lines are low angle grain boundaries (LAGBs) and black lines are high-angle grain boundaries (HAGBs).

4.2 Microstructures of reversed structures

4.2.1 Definitions of the microstructural features

The reversion-processed structures consisted of reversed austenite (RA) with different GSs and possibly some DIM as a retained phase, depending on the T_p (and the annealing duration) after high (63%) CR reduction. The following reversed structures were found and discussed in the studies (Papers I–VI):

A *coarse-grained austenite* (CGA) structure was created in reversion annealing at temperatures of 1000 °C and above. The CGA also consists of cold-rolled austenite grains that did not recrystallize (at temperatures of 800 °C and below) but remained as recovered during annealing (called deformed austenite; DA), and

shear-reversed austenite (SR), formed from DIM by a shear mechanism. The GS of the CGA was typically 20 μm , but all austenite grains with a GS larger than 10 μm were defined as CGA.

A *fine-grained austenite* (FGA) structure was created during short reversion annealing at a temperature around 900 °C. This GS was typically about 2 μm .

An *ultrafine-grained austenite* (UFGA) structure was created during short reversion annealing around 800 °C. The GS was typically below 1 μm and therefore these grains were also called *submicron-grained* austenite.

A *partially reversed austenite* (PRev) structure was created in short annealing at temperatures of 750 °C and below. The structure contained retained DIM in addition to austenite with various GSs. The GS distribution of reversed austenite was similar to that of the UFGA structure.

In the studies on the effect of low CR reduction on the reversed structures in Paper V, in addition to the above general structures, a classification of local GSs was adopted. In this classification, so-called *fine-sized austenite* (FSA) and *medium-sized austenite* (MSA) grains in addition to coarse grains were termed to classify the different GSs existing locally in the above-mentioned structures. The GSs of the MSA were defined to be in the range of 3 to 10 μm to distinguish them from finer (FSA) and coarser austenite grains existing simultaneously. The FSA was formed from highly deformed DIM, whereas the MSA was formed from slightly-deformed DIM, DA and reversed austenite at temperatures below 1000 °C. Typical examples of the above microstructures are displayed in Fig. 4.

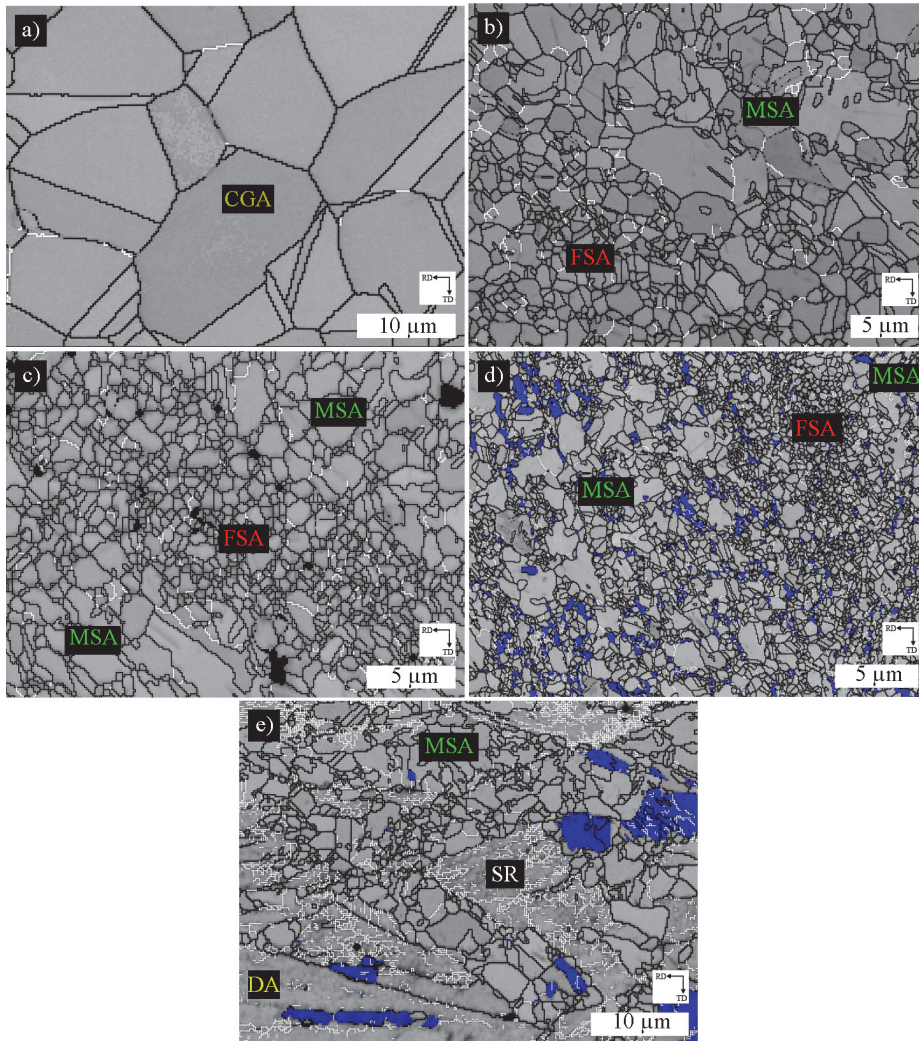


Fig. 4. Typical reversed structures showing (a) coarse-grained austenite (CGA) formed at 1000°C, (b) fine-grained austenite (FGA) formed at 900 °C, (c) ultrafine-grained austenite (UFGA) formed at 800 °C, (d) partially reversed austenite (PRev) formed at 750 °C, all after 63% cold rolling reduction and (e) PRev formed at 750 °C after 32% cold rolling reduction. EBSD grain boundary maps overlapped with phase maps. Austenite = grey and DIM = blue. FSA = fine-sized, MSA = medium-sized, SR = shear-reversed and DA = deformed austenite. White lines are low angle grain boundaries, black lines are high angle grain boundaries, unindexed pixels are black. (Reprinted by permission from Paper III © 2017 Elsevier).

4.2.2 Phase structures

As evident from Fig. 4, the annealing temperature has an important impact on the detailed features of the reversed structures. At a high T_{ps} (800 °C and above after 63% CR) complete reversion can occur, while all of the DIM transforms to CGA (Fig. 4a) or FSA grains (FGA in Fig. 4b and UFGA in Fig. 4c) and DA recrystallizes to MSA or CGA grains. Partially reversed structures formed at lower temperatures are even more complex, consisting of various amounts of retained DIM and DA, dependent on the amount of CR reduction, in addition to new austenite with various GSs (Figs. 4d and 4e). The phase (DIM, DA and RA) fractions of the studied reversed structures are listed in Table 4.

The effect of CR reduction on the reversed microstructures was investigated in Paper V. CR reduction had a distinct effect on the refinement of GS, as will be shown in the next section. The degree of CR also strongly affected the DA fraction (Fig. 2, Table 4) and the texture of the reversed structure (Section 4.2.4). As in the cold-rolled structures (Fig. 3), DA grains appeared as large stretched/pancaked grains ($GS > 10 \mu m$), but sometimes also as narrow bands a few micrometres wide among the DIM. Austenite grains that were only partially transformed to DIM were typically seen in highly cold-rolled 56CR (Fig. 3c) and 63CR structures. Some DA grains exhibited recrystallized bands after low-temperature reversion treatment.

Table 4. Phase fractions of the studied structures based on XRD measurements.

| Code | Structure | DIM | DA | New austenite |
|---------------|-----------|-----|----|---------------|
| 32CR-750-0.1 | PRev | 9 | 30 | 61 |
| 63CR-750-0.1 | PRev | 2 | 4 | 94 |
| 32CR-690-70 | PRev | 9 | 30 | 61 |
| 56CR-690-60 | PRev | 2 | 5 | 93 |
| 63CR-800-1 | UFGA | ~0 | ~0 | ~100 |
| 32CR-900-1 | FGA | 0 | 0 | 100 |
| 63CR-900-1 | FGA | 0 | 0 | 100 |
| 63CR-1050-200 | CGA | 0 | 0 | 100 |

4.2.3 Austenite grain sizes

Austenite exists in grains with various sizes in the reversed structures. The fractions of the GS classes are listed in Table 5. The T_p had a significant effect on the AGS of the reversed structure. It is seen that finer AGSs were attained at lower T_p s, as also shown in many previous papers (Huang, Ye, et al., 2012; Misra, Nayak, Mali, Shah, Somani & Karjalainen, 2010; Misra, Zhang, Venkatasurya, et al., 2010; Rajasekhara et al., 2007; Takaki et al., 1994; Tomimura, Takaki, Tanimoto & Tokunaga, 1991). However, nano-scale GSs can hardly be reached in processing such as was presently employed (Misra, Nayak, Mali, Shah, Somani & Karjalainen, 2010; Misra, Zhang, Venkatasurya, et al., 2010). Also, the impact of CR reduction on AGS was considerable. AGS based on the HAGBs was 1.2 and 0.6 μm in the partially reversed structures of 32CR-750-0.1 and 63CR-750-0.1, respectively.

Table 5. Fractions (in per cents) of different austenite grain size classes in the reversed structures, calculated as a fraction of area, and average grain size (AGS in μm) as a number frequency. FSA grains with a GS < 3 μm , MSA grains with a GS = 3–10 μm and CGA grains with a GS > 10 μm .

| Code | Grain size class | | | AGS |
|---------------|------------------|-----|-----|-----|
| | FSA | MSA | CGA | |
| 32CR-750-0.1 | 21 | 41 | 30 | 1.2 |
| 63CR-750-0.1 | 76 | 18 | 4 | 0.6 |
| 32CR-690-70 | 23 | 34 | 35 | 1.2 |
| 56CR-690-60 | 67 | 28 | 5 | 0.7 |
| 63CR-800-1 | 69 | 28 | 3 | 0.6 |
| 32CR-900-1 | 8 | 70 | 22 | 3.4 |
| 63CR-900-1 | 64 | 33 | 3 | 1.4 |
| 63CR-1050-200 | 0 | 9 | 91 | 20 |

It must, however, be realised that AGS is not an adequate measure for characterising the properties and stability of reversed structures, as the GSs were generally quite non-uniform. Roughly, two types of reversed areas with FSA and MSA grain classes (Figs. 4b and 4c) could be distinguished, as patches in the sheet surface views or as bands in the cross-sections, where in addition to the degree of deformation of DIM, chemical inhomogeneity also had some impact (see Papers I and III). Furthermore, depending on the T_p and the degree of CR reduction, the reversed structures also contained varying fractions of CGA grains. The GS distributions were presented for various structures in Papers I and V. It was noticed that the 63CR-750-0.1 structure consisted mainly (76%) of FSA grains, whereas

the 32CR-750-0.1 structure, which has a high fraction of coarse non-recrystallized DA and MSA grains, only had 20% FSA grains. The increase in the T_p increased the MSA fraction and decreased the FSA fraction, whereas the fraction of CGA decreased due to recrystallization of DA grains.

4.2.4 Texture of low-temperature reversed structures

The orientation of grains affects their stability (Poulon, Brochet, Glez, Mithieux & Vogt, 2010), so it is important to examine the orientation of different GSs to understand the features affecting the stability of low-temperature reversed structures. The textures of the studied structures were examined by XRD and EBSD and the results are published in Papers I and III. It is seen from the XRD-ODF plots (Fig. 5) that the CGA grains (Fig. 5a) were randomly oriented, but the reversed structures exhibited texture. A weak Goss component was present in the FGA structure (Fig. 5b), whereas in the UFGA (Fig. 5c) and PRev (Fig. 5d and 5e) structures the austenite texture consisted of a major Brass and a minor Goss component, which became intensified with decreasing T_p (from 800 °C to 700 °C). The retained DIM showed the main $\{112\}$ $\langle 110 \rangle$ and $\{554\}$ $\langle 225 \rangle$ texture components, i.e. α -fibre from the CR, $\langle 110 \rangle$ direction parallel to the RD, and shifted γ -fibre. As a further detail, Fig. 6 shows the strong Brass orientation of recovered DA and shear-reversed grains in the partially reversed 63CR structure. The Brass component was also more likely to be observed among submicron-grains than in larger reversed grains.

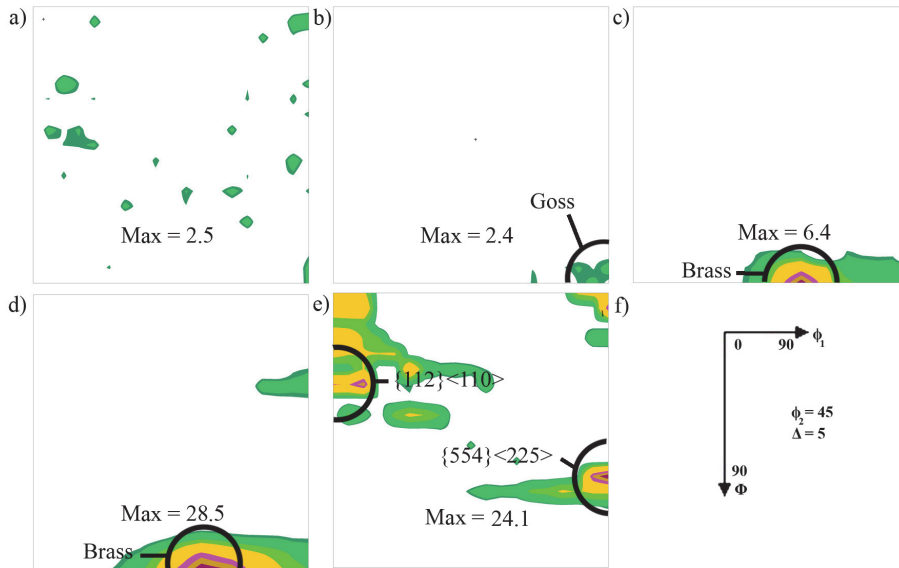


Fig. 5. Typical texture components of reversion-treated 63CR structures (from the cross-sections) shown in XRD-ODF ($\phi_2 = 45^\circ$ section) plots for (a) coarse-grained, (b) fine-grained, (c) ultrafine-grained, (d) partially reversed (fcc) and (e) partially reversed (bcc) structures. (Reprinted by permission from Paper I © 2017 Elsevier).

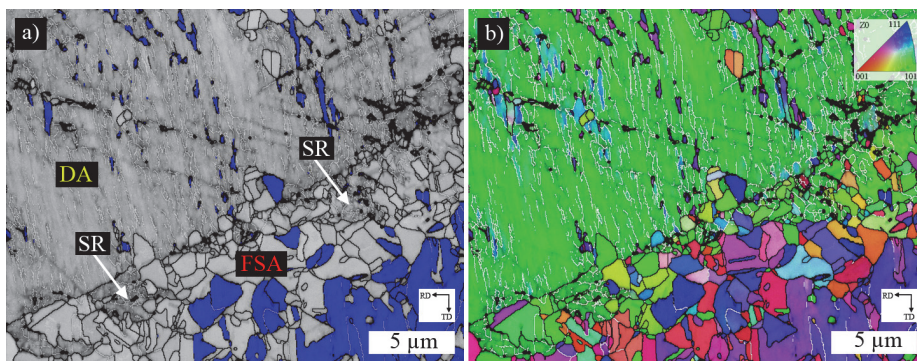


Fig. 6. EBSD grain boundary maps overlapped with (a) phase and (b) IPF maps showing the complex features of the partially reversed structure (63CR-750-0.1). SR grains indicated by arrows in (a). Phases with different colours: austenite = grey and DIM = blue. FSA, DA and SR austenite grains. White lines are LAGBs, black lines are HAGBs. (Reprinted by permission from Paper I © 2017 Elsevier).

4.3 Mechanical stability of reversed structures

To explain the mechanical stability of the complex microstructures created at low reversion temperatures, the microstructures were carefully characterised by EBSD during both tensile and cyclic straining (Papers I–VI). Especially the effect of different types of austenite phases (DA and RA), the GS of RA and the texture of DIM formation were emphasised. Loading in both the monotonic and cyclic tests was mainly directed transversely to the rolling direction (TD), but some structures were also tested under loading parallel to the rolling direction (RD). The effect of the loading direction on austenite stability under monotonic straining was highlighted in Paper I. In general, austenite stability is higher when loaded in the TD direction.

The present study shows that the reason for the reduced stability of low-temperature reversed structures is not the submicron GS, as argued in some prior works (Behjati et al., 2014; Kisko et al., 2013; Maréchal, 2011; Somani et al., 2009). In fact, the stability of the finest grains is high, but the stability of low-temperature structures is significantly decreased by nitride precipitation, as is considered in Section 5.2.2.

4.3.1 Mechanical stability under monotonous deformation

Tensile true stress-true strain and strain hardening rate (SHR) curves were determined (Fig. 7) and related to the evolution of DIM (Fig. 8) (Papers I, IV, V). All the curves in Fig. 7a reveal a concave shape; less hardening under small strains followed by an increasing hardening rate. Even a characteristic plateau resembling the Lüders strain appears in the flow curves of the partially reversed structures, although it is seen more prominently in engineering stress-strain curves (an example is shown later in Fig. 22). The SHR curves (Fig. 7b) exhibit a deep drop in the SHR – even softening of 63CR-750-0.1 – followed by a rapid increase in the SHR before the final descending stage. The peak SHR is seen at approximately 0.15 true strain in all the low-temperature reversed structures, whereas it occurs at approximately 0.25 in the other structures, indicating lower stability in the low-temperature structures compared with the other counterparts. The maximum SHRs did not vary much in the reversed structures, except in 32CR-750-0.1; the strongest structure contained 30% DA without recrystallization, which clearly showed a lower and broader curve shape at the peak regime. Correspondingly, the highest SHR value was recorded in 63CR-1050-200, the softest structure.

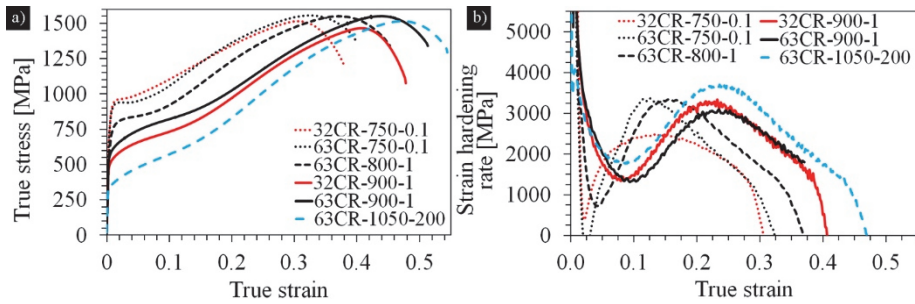


Fig. 7. True stress-true strain curves (a) and strain hardening rate curves (b) of the reversed structures; loading in the TD direction. (Reprinted by permission from Paper III © 2014 Elsevier, reprinted by permission from Paper V © 2018 MDPI).

The evolution of the DIM fraction and the transformation rate of martensite, i.e. austenite stability, was measured by interrupting the tensile tests under various preselected strains without unloading the specimens (Papers I, II and IV). The DIM fractions plotted in Fig. 8 were measured at the surface layer, and the average value from two specimens is given. Similar measurements were also carried out by unloading the specimens (e.g. in Paper V). Then it was noticed that the DIM fraction measured without unloading was lower than that determined from unloaded specimens (Beese & Mohr, 2011). The unloaded specimens saturated at nearly a 100% DIM fraction under the highest strains. However, the trend and order between the structures were otherwise independent of the measurement technique.

It was seen that a decrease in the T_p from 900 to 750 °C lowers the tendency for DIM transformation significantly at both CR reductions. DIM formation began at lower strains in the low-temperature reversed structures (750 and 800 °C) and the peak transformation rate was higher than in the structures created at 900 °C. For instance, the 32CR-750-0.1 structure showed both the earliest increase and decrease in the transformation rate, although the final DIM fraction roughly equalled that observed in the 32CR-900-1 structure. Later, this difference will be linked to precipitation occurring at a low T_p s.

The impact of CR reduction can be noticed by comparing the reversed 32CR structures with the 63CR counterparts, and in all cases, at a given T_p 32CR reduction resulted in a structure with lower stability than 63CR reduction did. The main difference caused by CR reduction in the completely reversed structures obtained at 900 °C is in GS distribution (Table 5). The 32CR-900-1 structure has 92% MSA grains, whereas the 63CR-900-1 structure consists mainly of FSA grains,

suggesting an important contribution of MSA grains in reducing austenite stability. The difference in stability is not as pronounced in the 750-1 structures, although distinct under small strains. Correspondingly, there is a difference in the fraction of MSA grains.

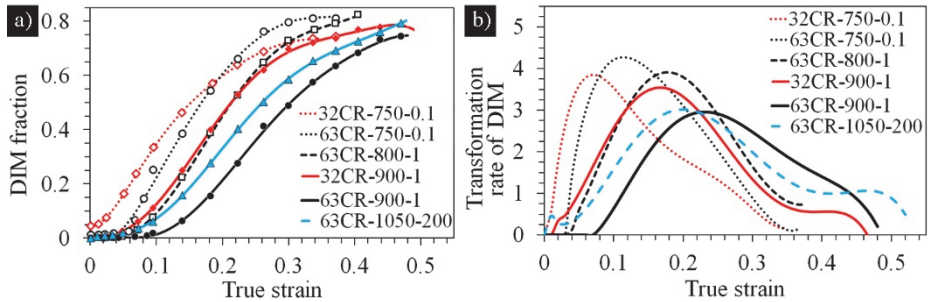


Fig. 8. Evolution of the deformation-induced martensite fraction (a) and the transformation rate (b); loading in the TD direction. (Reprinted by permission from Paper III © 2014 Elsevier, reprinted by permission from Paper V © 2018 MDPI).

4.3.2 Cyclic and mechanical stability under fatigue loading

The fatigue behaviour of the low-temperature reversed structures was studied under stress- and strain-controlled fatigue cycling (loaded mostly in the TD direction). It was first shown under pull-pull load-controlled experiments (Paper II) that the low-temperature reversed 63CR structures produced higher amounts of DIM at a very early stage of cycling than the high-temperature 63CR-1000-100 structure did. Due to the testing condition, relatively high plastic strains ($\sim 10\text{--}20\%$) occurred within the first few cycles in these experiments.

In a more extensive study, the stability of the structures in strain-controlled fatigue tests was investigated (Papers III and VI), where low strain amplitudes were applied to the structures. The evolutions of stress amplitude (cyclic stability) and DIM fraction (mechanical stability of the austenite) were recorded at various total strain amplitudes (ϵ_{at}). It was noticed that the low-temperature reversed structures did not exhibit changes in stress amplitude (σ_a) at a low ϵ_{at} of 0.3% (Fig. 9a). In the softer high-temperature 32CR-900-1, 63CR-900-1 and 63CR-1050-200 structures, where a higher plastic strain component existed, faint cyclic softening could be noticed. At higher ϵ_{at} s (Fig. 9c), all the structures showed unstable behaviour, where initial slight cyclic softening was followed by a pronounced hardening period. The low-temperature reversed structures exhibited the lowest amounts of cyclic

softening. Also, there was less cyclic hardening in these structures. Contrarily, cyclic hardening was much more prominent in the soft structures created at 900 and 1050 °C, which had a low initial stress amplitude.

The 32CR structures were mechanically more stable than the 56CR and 63CR counterparts. The difference in stability is seen as a higher initial stress amplitude, but a lower final stress amplitude in the 32CR structure (Fig. 9c).

As seen in Figs. 9b and 9d, DIM transformation occurred over the course of cycling after certain incubation periods. At a ϵ_{at} of 0.4%, some DIM could be formed simultaneously with the occurrence of slight softening. DIM formation became more pronounced at a higher ϵ_{at} of 0.6%, while cyclic hardening also took place. It is quite evident that cyclic hardening and DIM formation coincide. The amount of DIM formation was quite similar among the other studied structures, except that it was lower in the 900-1 structures, independently of CR reduction.

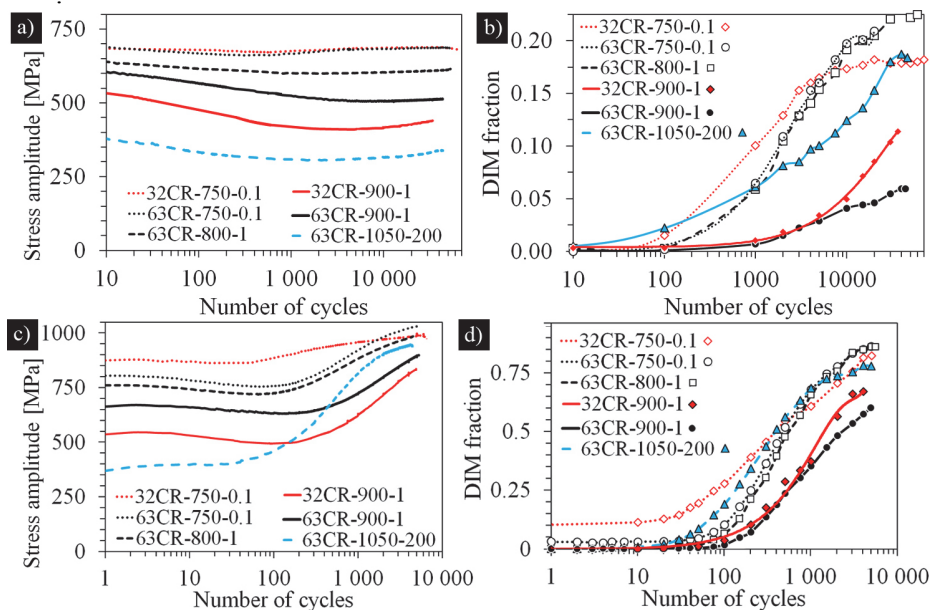


Fig. 9. Evolution of stress amplitude (a,c) and DIM fraction (b,d) at strain amplitudes of 0.4% (a,b) and 0.6% (c,d) in various structures. (Reprinted by permission from Paper III © 2014 Elsevier).

4.3.3 Martensite nucleation under tensile straining

To identify the most unstable grains under monotonous straining, DIM nucleation sites in completely and partially reversed structures were examined by interrupting tensile tests after various strains for EBSD analysis (Papers I and V). Examples of typical microstructural features in the surface layers of the sheets after 0.10 true strain of completely reversed 63CR-800-1 and 63CR-900-1 (FSA+MSA, Table 5) structures are shown in Fig. 10a and 10b, respectively. Deformation bands were not found in these structures and DIM seemed to nucleate preferably inside or at the grain boundaries of MSA grains, not within FSA grains. In the CGA structures of 63CR-1050-200 and Com-301LN, martensite tended to nucleate at deformation bands (see Fig. 10c as an example) and at grain boundaries.

In the partially reversed structures, most of the DIM was also formed in MSA grains (Fig. 10d). Additionally, some DIM was detected in DA grains as tiny grains along deformation bands. Generally, the DA grains were very stable even though they were coarse in size. This is explained by their strong Brass-type orientation (green colour in Fig. 10e), but possibly also because they were harder than the MSA grains while more strain was concentrated in the MSA grains (Paper V). Also in XRD analysis, the intensity of the Brass component of the austenite was found to increase in monotonic deformation, i.e. DIM formation was relatively lower in the Brass-oriented grains (Papers I and III).

Even though local variations in the DIM fraction were high, a distinct difference between the amount of DIM in the 63CR-800-1 and 63CR-900-1 structures can be seen in Figs. 10a and 10b. As shown earlier in Fig. 8a, the DIM fraction in the latter structure was systematically significantly lower at small strains than in the low-temperature reversed structures. This happened in spite of the higher fraction of MSA grains present in the 63CR-900-1 structure than in the 63CR-750-0.1 or 63CR-800-1 structures (Table 5). This indicates that the T_p has a more significant impact than GS on stability.

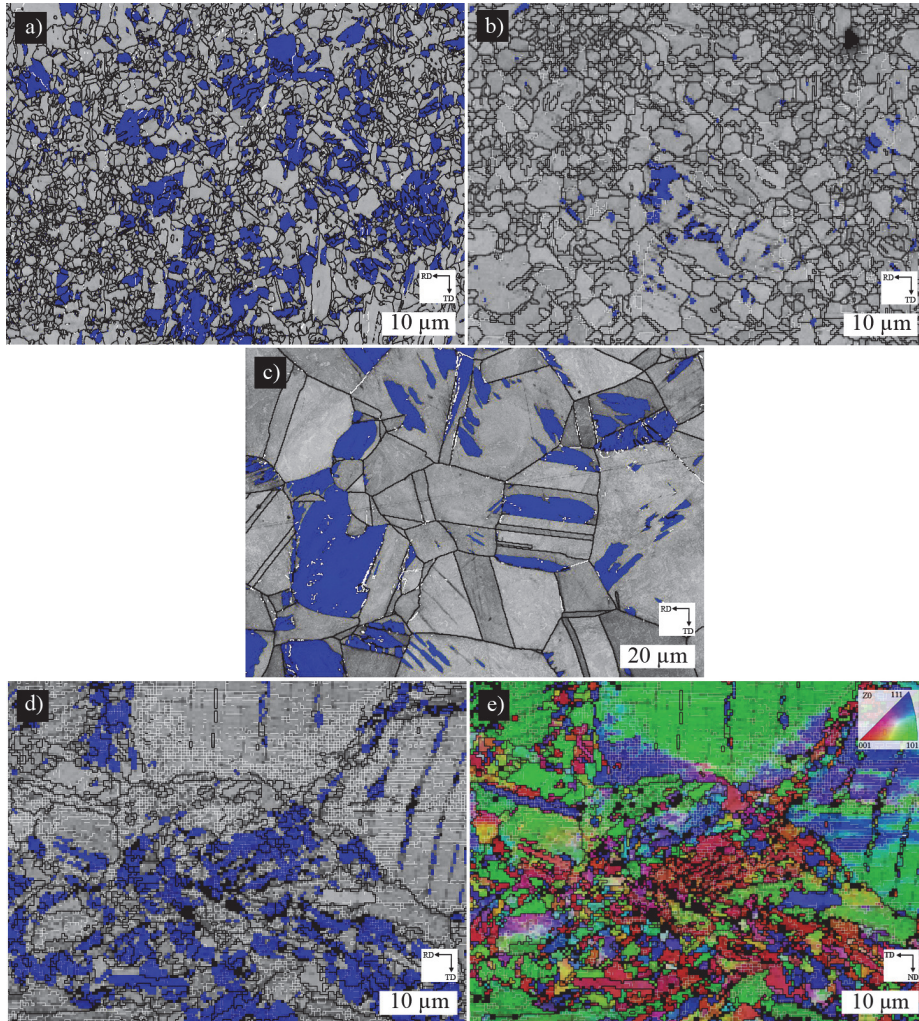


Fig. 10. Local DIM nucleation in medium-sized and coarse grains. A surface EBSD view of (a) 63CR-800-1, (b) 63CR-900-1 and (c) 63CR-1050-200 after 0.10 strain, and (c,d) 32CR-750-0.1 after 0.07 strain; loading in the TD direction. Different colours in the phase maps (a,b,c,d): Grey phase = austenite and blue = DIM. (d) An IPF map of (c). (Modified from Papers I and V).

4.3.4 Martensite nucleation under cyclic straining

The cumulative nature of the plastic deformation in the fatigue tests resulted in DIM nucleation similar to that observed under monotonic straining. It has to be pointed out that in this study, the strain rate applied was quite high and additional cooling was used to prevent the temperature of the specimens from rising. Yet some adiabatic heating might have occurred. The effect of the strain rate in fatigue testing has been characterised in a separate publication for the same structures giving such signs (Man et al., 2018). Thus, some concern about the reliability of the quantitative results may be raised, but the qualitative order of stability of the various structures seems to be correct.

The difference in stability between the low-temperature reversed structures and the 63CR-900-1 structure, observed in tensile testing, was present also under cyclic straining, as revealed by the data in Figs. 9b and 9d and also in Fig. 11. It is seen from Fig. 11 that the Brass-oriented grains, i.e. the greenish areas on the IPF maps, remained austenitic more likely than the grains with other orientations, which is consistent with the observation under monotonic straining. The SR (inserts in Fig. 11) and DA grains exhibited the highest stability, but also the greenish RA grains were resistant against DIM nucleation. DIM nucleation in the reversed structures occurred preferably in the MSA grains, but as highlighted in Fig. 11c and 11d, even these grains were stable if Brass-oriented. In summary, under monotonic and cyclic straining, due to their larger GS but also due to their generally random orientation, the MSA grains had a higher tendency to transform to DIM than the FSA grains had.

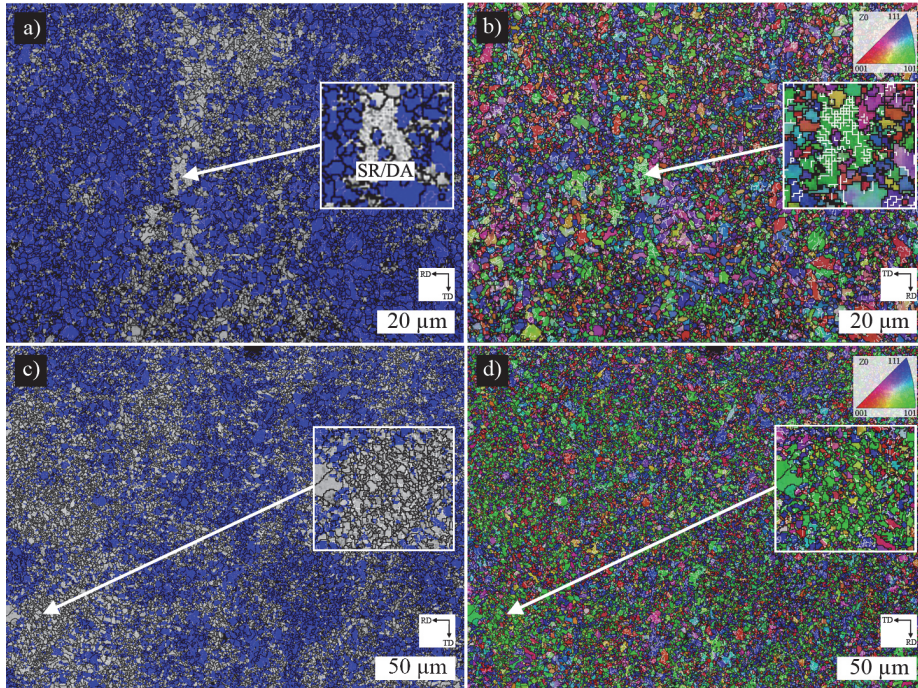


Fig. 11. EBSD maps showing DIM nucleation preferably in medium-sized grains in the 63CR-800-1 structure (a,b) and in the 63CR900-1 structure (c,d) after 5000 cycles at 0.6% total strain amplitude; loading in the TD direction. Inserts show the high stability of shear-reversed austenite (a,b) and Brass-oriented fine-sized grains (c,d). EBSD grain boundary maps overlapped with phase (austenite grey, DIM blue) (a,c) and IPF (b,d) maps. (Reprinted by permission from Paper III © 2017 Elsevier).

An example of DIM nucleation in an MSA grain is shown in Fig. 12. Six different DIM nuclei in a single grain $\sim 6 \mu\text{m}$ in size were found and numbered. The three different colours of the nuclei on the IPF map (Fig. 12b) indicate that they represent martensite variants with different orientations. In FSA grains, DIM typically possesses the form of a single block.

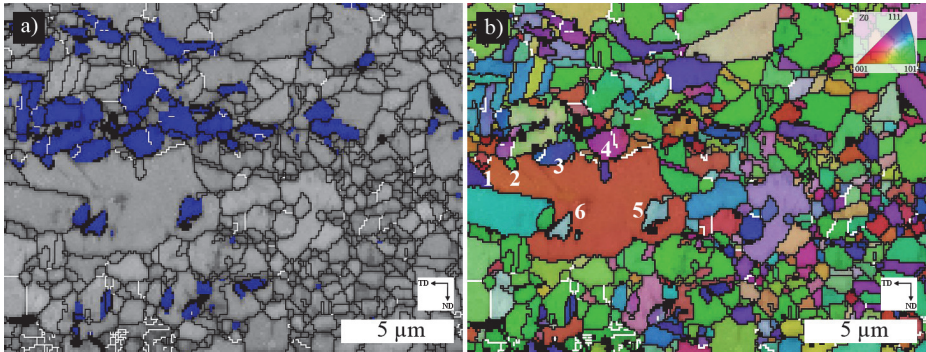


Fig. 12. EBSD grain boundary maps overlapped with phase (a) and IPF (b) maps revealing nucleation of DIM in the 63CR-800-1 structure after 44000 cycles at 0.4% total strain amplitude; loading in the TD direction. Six martensite nuclei in an MSA grain numbered in an IPF. (Reprinted by permission from Paper III © 2017 Elsevier).

4.4 Mechanical properties

The final engineering objective of reversion treatment to create refined structures is to improve mechanical properties. The tensile properties of this particular steel in reversed conditions have already been reported, e.g. by Somani et al. (2009), who found significantly enhanced strength-elongation combinations compared with commercial 301LN grade steel. Tensile and fatigue strength properties were not the main objective of the present work, but they were recorded; the main attention was focused on partially reversed low-temperature structures.

4.4.1 Tensile properties of reversed structures

Table 6 lists the tensile properties (3–6 repetitions) of the studied structures measured in the TD loading direction. Tensile properties were also determined in the RD direction, but there was little anisotropy (typically below 5%) and the results are not presented here for simplicity. Two different groups of structures can be identified based on tensile properties. Group 1 – low-temperature reversed structures – showed significantly enhanced yield strength (YS) and a distinct upper yield point (UYP), slightly higher ultimate tensile strength (UTS) and a minor decrease in ductility (~ 10%-units) compared with commercial steel. Group 2, consisting of structures created at temperatures of 900 °C or higher, showed lower

mechanical strength. Importantly, prior CR reduction in the studied range did not affect the mechanical properties of the low-temperature reversed structures.

Table 6. Tensile properties of the studied structures shown in the TD at a strain rate of 0.0005 1/s.

| Code | YS | UYP | UTS | UEI | TEI |
|---------------|-------|-----|------|-----|-----|
| | [MPa] | | | [%] | |
| 32CR-750-0.1 | 850 | 940 | 1130 | 31 | 46 |
| 63CR-750-0.1 | 840 | 925 | 1150 | 31 | 49 |
| 32CR-690-70 | 825 | 930 | 1180 | 30 | 49 |
| 56CR-690-60 | 820 | 900 | 1075 | 29 | 42 |
| 63CR-800-1 | 750 | 800 | 1100 | 31 | 49 |
| 32CR-900-1 | 490 | - | 990 | 47 | 61 |
| 63CR-900-1 | 550 | - | 1025 | 47 | 67 |
| 63CR-1050-200 | 360 | - | 965 | 52 | 71 |
| Com-301LN | 340 | - | 920 | 49 | 68 |

4.4.2 Cyclic strength of reversed structures

The data, although limited in number, from total strain amplitude-controlled fatigue tests were used to determine S-N curves (total strain and mid-life stress amplitudes vs. number of cycles to fracture) for the studied structures. The S-N curves for the Gleeble-treated and induction-treated specimens are plotted in Figs. 13a and 13b and Figs. 13c and 13d, respectively.

Commonly, the behaviour of a structure in a low cycle fatigue (LCF) regime (< 100 000 cycles) can differ from that in a high cycle fatigue (HCF) regime. In the fatigue tests, the HCF regime was reached at a ϵ_{at} of 0.3% with all the reversed structures, but a smaller ϵ_{at} (0.20–0.25%) was high enough for the coarse-grained reference structures (Figs. 13a and 13c).

As seen in Figs. 13a and 13c, LCF life is not significantly affected by the microstructure, a fact suggested by the Coffin-Manson relation (Cooper & Fine, 1984). However, the difference becomes obvious at lower ϵ_{atS} (< 0.4%) in the HCF regime, where the reversed structures showed better fatigue resistance than the coarse-grained Com-301LN (Fig. 13c). The same is valid also in a comparison based on mid-life stress amplitude (Figs. 13b and 13d), where the difference exits in the LCF regime, too. The cyclic stress levels followed the order in YS, but being mid-life values, they were also affected by the cyclic stability of the structure. A lower strain rate ($2 \times 10^{-3} \text{ s}^{-1}$) seems to enhance fatigue resistance slightly in a LCF

regime, as seen by comparing the data from (Chlupova, Man, Polák & Karjalainen, 2014) in Fig. 13a.

Fatigue strength, i.e. the stress amplitude level at 10^6 cycles, was in the range of 460–570 MPa in the reversed structures, being even more than double the corresponding values of the 63CR-1050-200 and Com-301LN structures (Fig. 13). The fatigue strength of the reversed 63CR structures was slightly dependent on the annealing parameters; the lower the T_p , the higher the fatigue strength at 10^6 cycles. It seems that low prior CR reduction can lead to fatigue strength equal to that achieved after 63% CR reduction, for the highest fatigue strength of over 500 MPa was obtained in the partially reversed 32CR and 56CR structures created at a lower T_p with a longer t_{ss} . The fatigue strength of the 32CR-690-70 steel was practically independent of the loading direction.

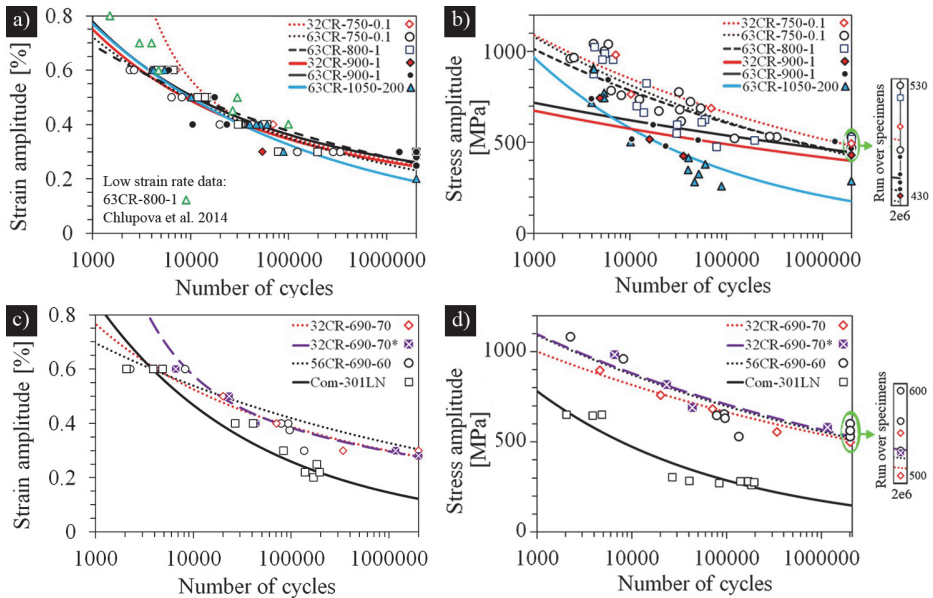


Fig. 13. Total strain amplitude vs. number of cycles to failure (a,c) and mid-life stress amplitude vs. number of cycles to failure (b,d). Upper figures, Gleeble-treated (TD direction) and lower figures, induction-treated (RD direction, except *) specimens. Note: The runover ($2e6$ cycles cut-off) specimens are shown in the inserts with a different y-axis scale. Own data from Papers III and VI. Low strain rate data in a) taken from (Chlupova et al., 2014).

4.4.3 The effect of subsequent cold rolling deformation on monotonic and cyclic strength of reversed structures

CR is commonly utilised to strengthen annealed austenitic stainless steels. Temper-rolled grades have an improved YS, though with decreased ductility and increased anisotropy (Karjalainen et al., 2008). The effects of rolling deformation on the mechanical properties of reversion-treated structures have not been investigated yet. A study (Paper VI) was done with specimens annealed using a semi-industrial induction line, where larger specimens than in a Gleeble could be heat-treated.

As seen from the list in Table 7, 10% CR reduction increased the YS of the 56CR-690-60 structure only faintly, although the DIM fraction grew by 10%. A 20% reduction increased the YS slightly more efficiently, but the improvement of 38% DIM was still very modest in comparison with the effect of the same CR reduction on soft Com-301LN steel by 29% DIM. It is obvious that the influence of DIM formation on strength is more pronounced in a soft CGA structure than in a strong reversed structure, but also the work-hardening of soft CGA must be much higher than the work-hardening of refined reversed grains, as will be discussed in Section 5.3.2. However, it can be noted that the partially reversed structure, without any additional strengthening, has practically equal YS and somewhat better elongation than those of the 20% cold-rolled commercial counterpart.

Table 7. Tensile properties and DIM fractions of commercial 301LN steel and 56CR-690-60 structures measured in the RD before and after strengthening cold rolling. (Reprinted by permission from Paper VI © 2014 Trans Tech Publications).

| Code | CR reduction [%] | DIM [%] | YS | UYP [MPa] | UTS | UEI [%] | Tel |
|-------------|---------------------|------------|-----|--------------|------|------------|-----|
| Com-301LN | 0 | 0 | 330 | - | 910 | 51 | 68 |
| | 10 | 5 | 560 | - | 1200 | 24 | 41 |
| | 20 | 29 | 800 | - | 1240 | 25 | 42 |
| 56CR-690-60 | 0 | 2 | 815 | 910 | 1105 | 32 | 45 |
| | 10 | 12 | 850 | 930 | 1250 | 20 | 32 |
| | 20 | 38 | 960 | - | 1360 | 15 | 27 |

Similarly, subsequent CR deformation had only a slight effect on the fatigue strength of the partially reversed structure, and the improvement was much more pronounced in the Com-301LN steel, as shown in Fig. 14. The partially reversed structures reached a fatigue life of 10^6 cycles at an approximately 0.3% strain amplitude in all conditions, similarly to the Com-301LN steel after 20% CR

reduction. Also, the stress levels at 10^6 cycles, determined from the fitting curves of the reversed structures and the 20% CR strengthened Com-301LN steel, were close to each other, about 600 MPa. The data taken from (Droste et al., 2018) for 17Cr-7Mn-7Ni steel shows a similar trend in fatigue resistance at a constant strain rate of $4 \times 10^{-3} \text{ s}^{-1}$ in the annealed condition. The UFG structure shows higher fatigue resistance; the stress levels in particular are clearly higher than in the CG condition (Fig. 14b). The calculated fatigue limit of the Cr-Mn-Ni UFG structure based on stress amplitude seems to be slightly higher than that of the 301LN steel.

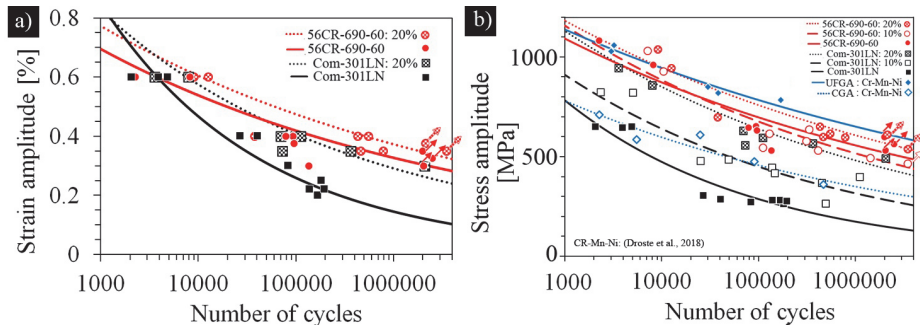


Fig. 14. The effect of subsequent rolling deformation on the fatigue strength of the reversed structure and commercial steel. Data for annealed Cr-Mn-Ni steel (Droste et al., 2018) is included. (Modified from Paper VI © 2018 Trans Tech Publications).

5 Discussion

As the primary results, complex microstructures were created by reversion annealing at low temperatures. They contained austenite grains of various sizes, depending on the degree of cold rolling reduction. These structures exhibited low stability against strain-induced martensite formation in tensile and dynamic loading and they had high strength and ductility as well as good fatigue strength even after prior 32% CR reduction. These characteristics and the influencing factors are discussed briefly in the following.

5.1 Low-temperature reversed structures

As described in the previous sections, the grain-refined reversed and partially reversed structures obtained by annealing at low temperatures of 800 °C or below are much more complex than simply consisting of reversed micron-scale grains. In fact, the UFGA structure created at 800 °C within 1 s contained recrystallized DA grains, coarse SR grains, dislocation-free MSA grains and submicron grains. Additionally, retained phases (recovered DA and DIM) were present in the partially reversed structures ($T_p \leq 750$ °C) in amounts dependent on prior CR reduction. A decrease in CR reduction was seen as broader GS distribution, increased AGS and a larger fraction of retained phases. In the present study, GS was classified into FSA, MSA and CGA, and particularly the significance of MSA grains was emphasised as regards the stability of austenite under straining.

5.1.1 Grain size distributions affected by annealing temperature and cold rolling reduction

As observed, austenite grains exist in various sizes in reversed structures. GS has an impact on strength, ductility and stability properties. A uniformly fine GS is often desired, even though the advantages of bimodal grain structures have been reported, especially for bcc steels, where ductility is limited due to ultrafine grains (Calcagnotto, Adachi, Ponge & Raabe, 2011; Lee, Lee & De Cooman, 2011). The classification of local GS was adopted earlier to point out the impact of MSA grains on the mechanical stability of austenite. Obviously, the three GS classes are a simplification of the structure; if we look at Fig. 15 that shows the GS distribution in detail in both number fraction and area fraction for various reversed structures.

At 800 °C (Fig. 15a), many DA grains are still not recrystallized or only partly recrystallized, which results in coarse grains among reversed ultrafine grains. In agreement with this, Rajasekhara et al. (2007, 2010) reported that particularly annealing at 800 °C for 1 s resulted in a broad GS distribution of a mixture of submicron grains and larger grains in 301LN steel. Similarly, Maréchal (2011) observed the same inhomogeneity in this steel type. Kisko et al. (2016) also showed that the microstructure of 204Cu steel annealed at 800 °C becomes non-uniform due to reversion of DIM – forming ultrafine grains – and recrystallization of DA grains, leading to coarser grains. At 900 °C, grain growth and complete recrystallization of DA grains can be expected to lead to a narrower GS distribution, but a larger AGS. The larger AGS can be seen in Table 5, but more uniform GS distribution is not yet so obvious after annealing at 900 °C, but is clearly seen at 1050 °C (Fig. 15e).

In this study, the effect of CR reduction on GS distribution was demonstrated using reduction as low as 32% (Figs. 15c and 15d). In fact, Di Schino, Barteri, & Kenny (2002) applied three reductions of 30%, 70% and 90% to 304-type steel, but they only report the beginning of reversion after 30% reduction during annealing at 750 °C for 1200 s. Takaki et al. (1994) have investigated the effect of CR reductions of 50% and 90% on reversion kinetics using TEM and have shown that an increase in CR reduction from 50% destroys the lath-like DIM structure into a cell structure and allows austenite grains to nucleate at random, leading to the formation of submicron-sized grains. At 50% CR reduction, a stratum structure with a coarser GS was observed.

In the present experiments, the influence of low CR reduction was seen as a larger AGS and the fraction of MSA grains in particular became pronounced when CR reduction was decreased from 63% to 32% (compare Figs. 14b and 14d). This is the result of an increasing fraction of low-deformed DIM and retained DA grains. In the same figures, the effect of large retained DA grains on the CGA fraction is also seen in the AGS range of 20–25 µm. The formation of submicron-sized grains in reversion is relatively clear, but the origin of the MSA grains is not as evident and special attention was paid to that.

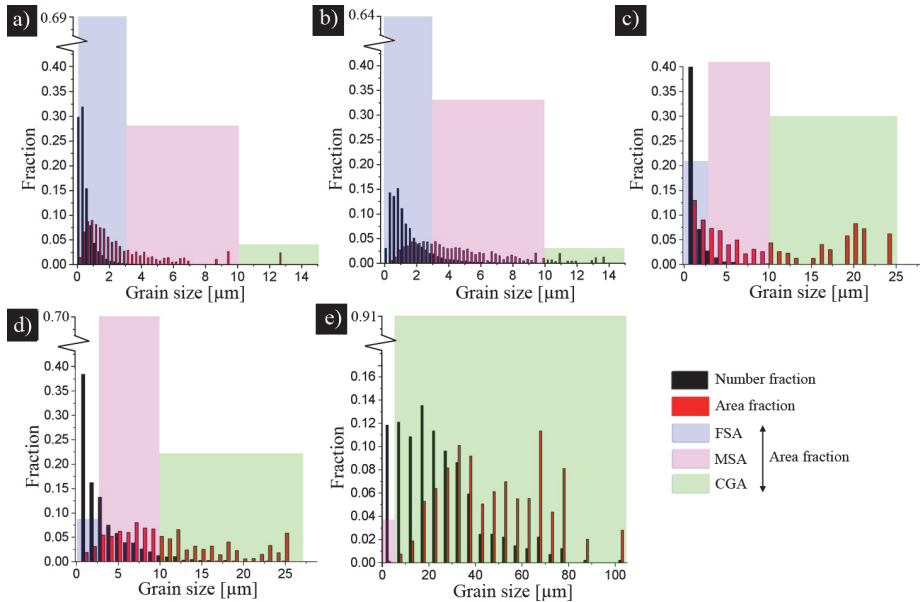


Fig. 15. GS distribution in the (a) 63CR-800-1, (b) 63CR-900-1, (c) 32CR-750-0.1, (d) 32CR-900-1 and (e) 63CR-1050-200 structures. (Modified from Papers I and V).

5.1.2 Formation of various austenite grain sizes in reversion

It was shown already in the beginning of the 1990s by Tomimura, Takaki, Tanimoto & Tokunaga (1991), Tomimura, Takaki & Tokunaga (1991) and Takaki et al. (1994) that submicron-sized austenite grains can form by diffusional reversion directly from DIM in cold-rolled austenitic steels (Misra, Zhang, Jia, Somani & Karjalainen, 2010; Misra, Nayak, Mali, Shah, Somani & Karjalainen, 2010). An increase in the degree of deformation of DIM decreases GS, but nucleation of larger MSA grains has not been accurately described. MSA grains could form directly from highly deformed DIM by diffusional reversion, but also from shear-reversed austenite or from DA. However, the fraction of DA is small in 56CR and 63CR structures, so it is not high enough to form MSA grains in any significant amount. Takaki et al. (1994) showed that in 18Cr–9Ni steel, after 50% CR reduction leading to slight deformation of DIM, the stratum structures of austenite laths and blocks were formed by a diffusional mechanism from a lath-martensitic structure. In the present case, the typical shape of the MSA grains was slightly flattened with multiple

corners (e.g. Fig. 16), so that they might resemble martensitic blocks. However, no substructure could be detected inside them.

To understand the origin of austenite grains with various sizes created at a low T_p s, the early stages of reversion were examined by heating the 32CR sheet to a low temperature of 700 °C for 0.1 and 1.0 s. The typical created microstructures are displayed in Fig. 16. Comparing these structures with the structure that existed after CR (Fig. 3), it is seen that the DA grains containing numerous LAGBs seem unchanged, but evidently new austenite grains have already appeared. The new grains seem to be formed by a diffusional mechanism, because they are free of substructures. In the 32CR-700-0.1 structure, the average fractions of new MSA and CGA grains were estimated as 6% and 55%, respectively, although the fractions varied significantly locally. Thus, the fraction of MSA grains was still low, but initially there was a distinctly higher fraction of CGA than DA grains (the fraction being only 30%). Thus, the amount of 25%-units of CGA must have formed from DIM. This must mean that shear reversion has also occurred, transforming some DIM to CGA.

Increasing the annealing duration to 1 s (Fig. 16b) or the temperature (Fig. 4e) significantly increased the fraction of MSA and decreased the CGA fraction in the 32CR structure. In principle, slightly deformed DIM, coarse DA grains and shear-reversed CGA grains can all be sites for formation of MSA grains during prolonged reversion. The decrease in the CGA fraction indicates that some of them have fragmented into finer MSA grains.

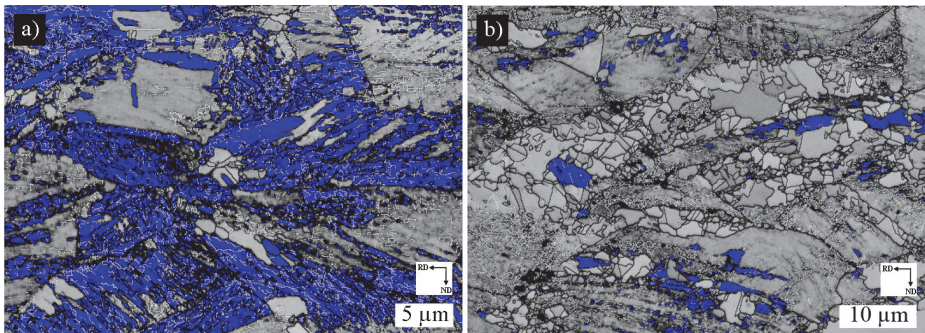


Fig. 16. Early stages of reversion in the 32CR-700-0.1 (a) and 32CR-700-1 (b) structures seen in EBSD grain boundary maps overlapped with phase maps. DIM = blue, austenite = grey and unindexed pixels = black. White lines are LAGBs and black lines are HAGBs. (Reprinted by permission from Paper V © 2017 MDPI).

Evidently, MSA grains form from shear-reversed austenite, as seen in Fig. 17. In the figure, large dislocated grains exhibit rearrangement of dislocations, creating a subgrain structure by the recovery process. Some subgrains adjacent to HAGBs first evolve to dislocation-free areas, which are separated later by an HAGB to form MSA grains (Paper V). The corresponding process has been suggested by Takaki et al. (1994), Tomimura, Takaki, Tanimoto & Tokunaga (1991), Lee, Oh, et al. (2008) and Ravi Kumar & Sharma (2014) based on TEM observations.

MSA grains might also form from DA grains, which when recovered resemble shear-reversed grains. However, the fraction of DA grains in 63CR and 56CR structures is very low compared with the MSA fraction (see Table 5), so DA grains cannot be a significant origin of MSA grains.

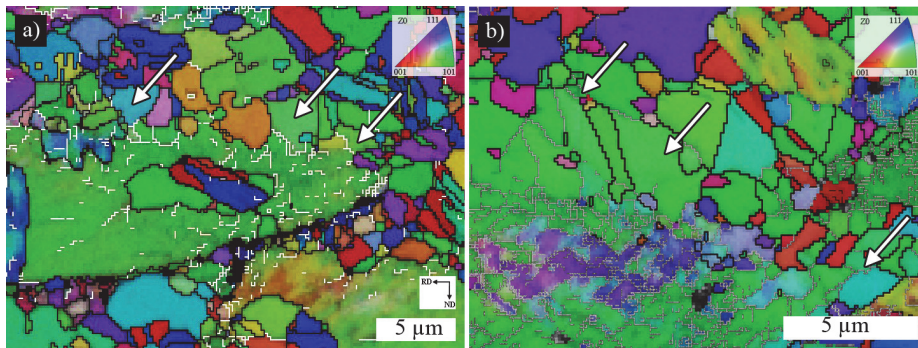


Fig. 17. Formation of medium-sized austenite grain from shear-reversed austenite by gradual evolution of subgrains in the 32CR-750-0.1 structure (examples shown by arrows). HAGBs are black lines and unindexed pixels = black, LAGBs are white in (a), grey in (b). (Reprinted by permission from Paper V © 2018 MDPI).

5.2 Stability of reversed structures

The results of the numerous experiments and microstructural examinations showed that the amount of deformation-induced α' -martensite (DIM) and its formation rate during monotonic and cyclic straining vary significantly between different microstructures in reversion-treated 301LN steel. These observations and the main factors that can be responsible for the change in stability detected between the structures are discussed in detail in the following.

5.2.1 The role of grain size

As presented in the Introduction, it is generally accepted that stability increases with decreasing GS. The data collected from the present study (Paper I) and Maréchal's work (2011) with 301LN steel also show a systematic trend between austenite stability and AGS in the range from 30 μm down to about 1 μm (Fig. 18). However, a few earlier works have demonstrated lower stability of submicron-sized grain structures as an exception in this relationship (Behjati et al., 2014; Kisko et al., 2013; Maréchal, 2011; Somani et al., 2009). Consistently, a steep drop in stability at GSs below about 1 μm is observed in the figure. A change in the nucleation mechanism of DIM in the submicron-sized austenite structure was suggested as a reason for the abrupt change in the trend (Kisko et al., 2013; Maréchal, 2011). However, it was realised in the present experiments (Sections 4.3.3 and 4.3.4) that the submicron-sized grains were relatively stable, similarly to the retained DA and SR grains. Instead, DIM formation occurred preferably in MSA grains (Figs. 10–12). The simplest explanation is that MSA grains are larger than submicron-sized grains and therefore more unstable. Dislocated CGA grains are stable due to their special orientation and strain distribution.

The fraction of MSA grains depends on the T_p and CR reduction, so we can expect stability to be affected by these processing factors. For instance, the MSA fraction in the 63CR-800-1 structure was approximately 50% higher than in the 63CR-750-0.1 structure and twice as high in the 32CR-900-1 structure as in the 63CR-900-1 structure. It was consistently found and shown that in these counterparts, the structures containing a higher fraction of MSA grains had lower austenite stability (Section 4.3). However, the drastic effect of the T_p between “low” temperatures ≤ 800 °C and 900 °C on stability cannot be explained by GS distribution. The effect of precipitation on the chemical composition of the austenitic matrix has to be taken into account, as discussed in the following.

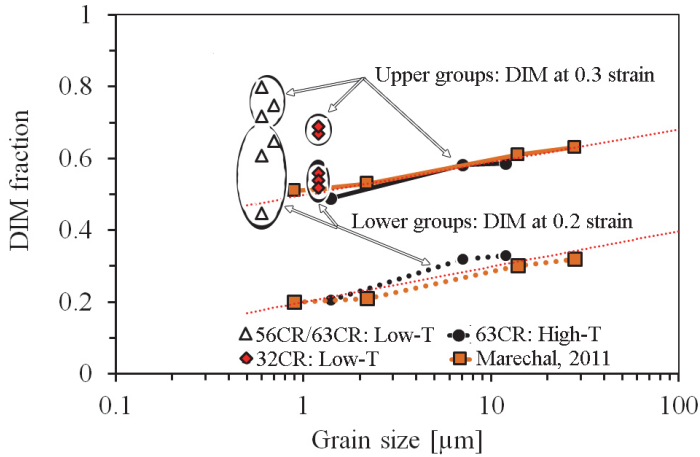


Fig. 18. The amount of new DIM formed under monotonic straining at 0.2% and 0.3% true strains as a function of average grain size. Low-T = $T_p \leq 800 \text{ }^\circ\text{C}$ and High-T = $T_p \geq 900 \text{ }^\circ\text{C}$. Own data from Papers I, V and VI. Maréchal's data from (Maréchal, 2011).

5.2.2 The role of precipitation

The observations revealed a distinct difference in austenite stability between the structures created by annealing at $800 \text{ }^\circ\text{C}$ or below and those annealed at $900 \text{ }^\circ\text{C}$ under monotonic loading as well as cyclic loading. Precipitation of chromium carbides and nitrides is possible in austenitic stainless steels (Simmons et al., 1996), so the impact of this process must be assessed. Martins, Plaut & Padilha (1998) showed that carbide precipitation in type 304 and 304L steels decreased both stability and strain hardening rate under rolling deformation. Somani et al. (2009) suggested that the reason for the lower stability of the UFGA structure formed at $800 \text{ }^\circ\text{C}$ compared with the structure formed at $900 \text{ }^\circ\text{C}$ in type 301 and 301LN steels under tensile deformation could be precipitation: carbide precipitation in 301 and nitride precipitation in 301LN steel. Precipitation could create local regions with depleted concentrations of stabilising elements, e.g. carbon and nitrogen. However, Somani et al. paid no further attention to this issue.

An extensive discussion was presented in Paper IV on the various mechanisms possibly affecting austenite stability. Consequently, it was argued that the primary mechanism leading to the reduced stability of the structure is precipitation, which occurs at low reversion temperatures but is absent at temperatures of $900 \text{ }^\circ\text{C}$ and above. To confirm this, experiments were conducted to find out if the high stability

of the structure formed at 900 °C would change as a result of annealing at lower temperatures. Indeed, the results indicated that the stability of the 63CR-900-1 structure decreased with prolonging subsequent annealing at 750 °C and reached the same stability as the 63CR-800-1 structure after 1000 s (Fig. 19). Annealing at 850 °C did not reduce stability much, so the phenomenon was absent at temperatures above 850 °C.

It can readily be argued that precipitation takes place at temperatures around 750–800 °C, leading to the observed drop in austenite stability. In agreement with the present results but reported later, He, Wang, Guo & Wang, (2017) have noticed drastically lower stability in the low-temperature (800 °C) reversed structure of type 321 (17Cr-8Ni-0.3Ti) steel compared with the structure formed at 1000 °C, in spite of the much finer GS of the former (GS 2.3 and 16 μm, respectively). The reason for the low stability was suggested to be carbide precipitation depleting austenite stabilising elements in the matrix. Kisko et al. (2013, 2016) have reported that prolonged annealing at 700 °C for 1000 s decreased the stability of type 204Cu steel. The reason for the reduced stability was not clarified, however, but we can now assume that carbide and nitride formation is behind the decrease in stability.

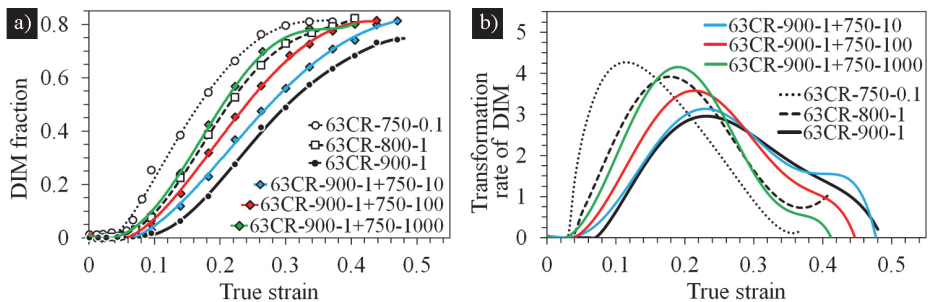


Fig. 19. Evolution of the DIM fraction in the precipitation-treated 63CR-900-1 structure after subsequent annealing at 750 °C for 10, 100 and 1000 s (coding +Tp-ts). (Modified from Papers I and IV).

The presence of precipitate particles was also confirmed in the matrix of the 63CR-900-1+750-1000 structure by STEM examinations, which revealed particles similarly to those reported by Rajasekhara et al. (2007, 2010) during reversion annealing of 301LN steel. The particles were identified as Cr₂N (Fig. 20), whereas Rajasekhara et al. reported the particles as CrN. The precipitation and its kinetics in 301LN were also modelled using ThermoCalc and Prisma software (Paper IV). Based on the calculations, Cr₂N precipitation occurs below 850 °C and the

maximum rate occurs at around 800 °C. The precipitation starts then within a few seconds and continues 1000 s or longer. Accordingly, the kinetics fits very reasonably with the experimental observations of progressively decreasing stability during annealing at 750 °C for 10–1000 s. This suggests that binding of nitrogen by precipitation of CrN or Cr₂N would be the reason for reduced stability in the structures formed at temperatures of 800 °C and below. It must be noted that in the experiments above, the precipitation took place in annealed austenite, whereas during reversion annealing it presumably occurs in deformed bcc-martensite before transformation, so the precipitation rate is much faster.

Hence, it can be argued that the major factor controlling austenite stability in the present N-bearing steel is the T_p , leading to very rapid precipitation of nitrides during low-temperature reversion. GS and texture are secondary factors affecting stability.

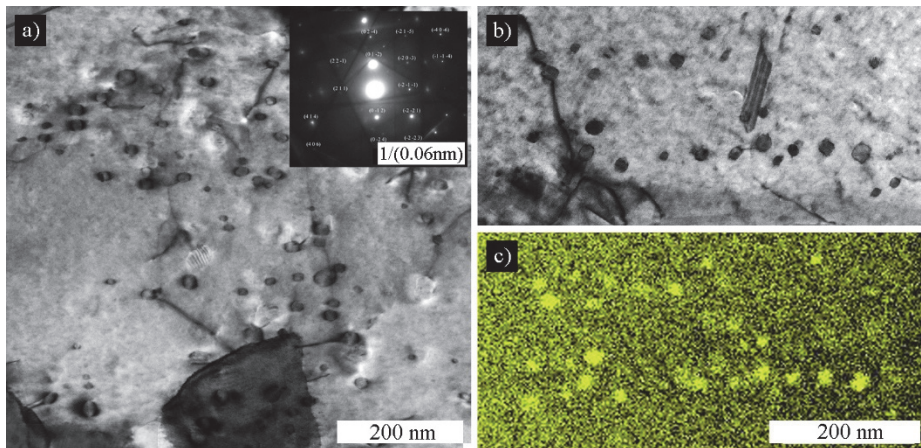


Fig. 20. STEM images of the 63CR-900-1 structure after subsequent treatment (750 °C for 1000 s), showing precipitation (a) inside a grain (insert of a typical nanobeam diffraction pattern of a Cr₂N-type particle, the zone [472]), (b) in rows and (c) enrichment of Cr. (Reprinted by permission from Paper IV © 2017 MDPI).

5.3 Mechanical properties of reversed structures

The study showed that equivalent properties can be obtained by low-temperature reversion with prior CR reductions in the range of 32–63%, though the GS distribution and phase structures exhibit distinct differences especially in the partially reversed (PRev) condition. The softness of the coarser RA grains in 32CR-

PRev was obviously “compensated” by the higher fraction of harder retained phases and shear-reversed austenite, and neither ductility nor fatigue strength were impaired by the complex microstructure. In the low-temperature reversed 56CR and 63CR structures, the good properties resulted mainly from efficient grain refinement. In the following, some aspects of tensile strength, strain hardening capability and dynamic behaviour among the low-temperature reversed structures are discussed.

5.3.1 Yield strength enhancement by refined grain size

The yield strength of the reversed structures is based mainly on the GS of new austenite, retained phases and their state, as well as on precipitation (Kisko et al., 2013; Martins et al., 1998; Rajasekhara et al., 2007; Somani et al., 2009). The complexity of the low-T reversed microstructures is the main reason for the scatter seen in the interdependence between yield strength and average grain size (Hall-Petch relationship), as observed by many authors (Fargas et al., 2015; Huang, Ye & Xu, 2012; Odnobokova, Belyakov & Kaibyshev, 2015; Rajasekhara et al., 2007; Ravi Kumar, Sharma, Kashyap & Prabhu, 2015). Some literature data reporting on 301LN steels were collected for comparison. As seen from Fig. 21, there is no unique Hall-Petch curve; especially the slope varies significantly. An obvious reason for the steeper slope is the presence of retained phases. For example, high fractions of DA and DIM were present in experiments carried out by Fargas et al. (2015) and Huang, Ye & Gu (2012), respectively, and their data show much steeper slopes. In the present study, a high YS of ~850 MPa was achieved with various microstructures containing either a high fraction of FSA grains with a small amount of retained phases (data points at $\sim 1.2 D^{-0.5}$) or a low fraction of FSA grains with a high amount of retained phases (points at $\sim 0.9 D^{-0.5}$). It was shown in Papers II and V that the hardness of the recovered DA was highest (about 400 HV), the hardness of the submicron-sized structure, medium (about 360 HV), and that of the MSA grains, lowest (about 300 HV).

Another factor affecting scatter is the non-uniform grain size, while AGS cannot describe the strength of the structure. The modified Hall-Petch relationship has been suggested to account for the grain size distribution (Lehto, Remes, Saukkonen, Hänninen & Romanoff, 2014).

The third feature affecting YS is precipitation at certain annealing temperatures. Rajasekhara et al. (2007) estimated the contribution of the various strengthening mechanisms and estimated 100 MPa as the amount of precipitation strengthening

after annealing at 800 °C. This analysis was not repeated here. In the present study, the precipitation treatment (Section 5.2.2) was experimentally found to increase the YS of the 63CR-900-1 structure by 40 MPa, but some decrease in elongation was observed. In Fig. 21, slightly higher YS values are seen for the low-T reversed structures, which could, however, be the result of several reasons, retained phases, non-uniform grain size and precipitation.

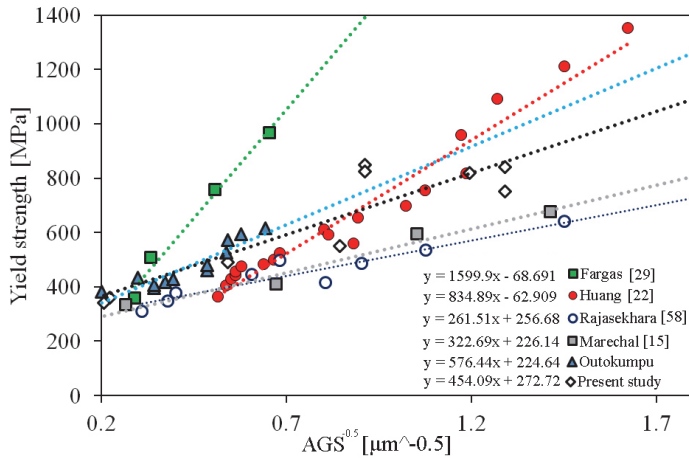


Fig. 21. Hall-Petch relationships for AISI 301LN steels revealing pronounced variation in slopes.

The effect of rolling deformation on YS was studied in a partially reversed 56CR-690-60 structure in Paper VI. For the first time it was shown that rolling deformation is an ineffective method for improving the YS of low-temperature reversed structures. This must mean that the work-hardening rate of grain-refined austenite with some retained phases is much weaker than that of conventional (soft) coarse-grained austenite. The weak strengthening by rolling may be related to the very low strain hardening (even softening) of certain reversed structures at small strains in tensile straining, as discussed in the following.

5.3.2 Yield point and low strain hardening in grain-refined structures

A typical particular feature of grain-refined structures seems to be prominent discontinuous yielding. This is evident in the stress-strain curves plotted in Fig. 22, where the Lüders strain can reach over 10% elongation (also seen in Fig. 7). As discussed by Song, Ponge, Raabe, Speer & Matlock (2006), a pronounced yield

point and a very long Lüders strain regime appear to be characteristics of ultrafine-grained steels and Al alloys. The appearance of a yield point with low subsequent hardening also happens in twinning-induced plasticity -type steels in connection with refinement of GS down to a few microns (Dini, Najafizadeh, Ueji & Monir-Vaghefi, 2010; Ueji et al., 2008). In the present study, a decrease in the T_p and an increase in CR reduction increased the Lüders strain and decreased the strain hardening rate. By comparing the 63CR-750-0.1 and 32CR-750-0.1 (Fig. 22a) or the 56CR-690-60 and 32CR-690-70 structures (Fig. 22b), it might be suggested that the difference in the Lüders strain and strain hardening capability are related to GS refinement and the fraction of the finest grains (Fig. 15). However, the differences in tensile behaviour between the reversed 63CR structures, for example, are not readily explained by GS distribution. In comparison with the 63CR-800-1 structure, initial softening became more pronounced in the structures created at 700 or 750 °C and the Lüders strain practically disappeared when the T_p was increased to 900 °C (Fig. 22a). This clearly seems to be connected to the AGS decreasing below one micron when the T_p decreases (Table 5). On the other hand, according to Fig. 15, the fraction of FSA grains (64–74%) is quite similar in these 63CR structures.

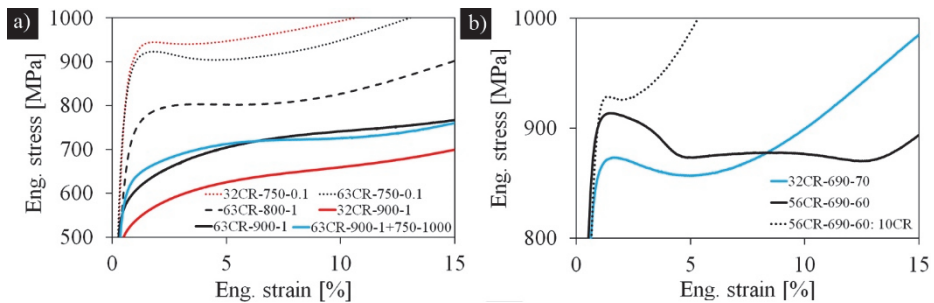


Fig. 22. Engineering stress-strain-curves for various reversed structures showing differences in yielding and strain hardening behaviour in loading (a) TD and (b) RD direction. 10CR = after subsequent 10% rolling deformation. (Modified from Paper VI).

Lüders-type behaviour has been detected in an Al-Mg-Li alloy in connection with precipitates (Wang & Prangnell, 2002), and in an ultrafine-grained Fe-C alloy with carbide particles (Lee, Park, Lee & Lee, 2011). Based on the results of the precipitation experiments (Section 5.2.2), the reversed the 63CR-900-1 structure created at 900 °C is free of precipitates and without a distinct Lüders strain. However, in subsequent annealing at 750 °C for 1000 s, strain hardening decreased,

although it remained positive (Fig. 22a). However, subsequent annealing could not refine GS, so a finer GS cannot be the sole reason for the change in yielding behaviour. Hence, we suggest that in addition to submicron-sized GS, the imposing softening and Lüders-type elongation are enhanced by the interaction between dislocations and fine precipitates, i.e. pinning effects. At any rate, the discontinuous yielding of a partially reversed structure can be largely diminished by subsequent 10% CR reduction, as shown in Fig. 22b. New dislocations are created by this plastic deformation.

In Section 4.4.3 it was reported that subsequent CR was ineffective in improving the YS of the reversed structures (Table 7), even though DIM was formed. The faint effect of DIM and deformation on the YS of the reversed structures compared with that on the YS of the CGA structures (63CR-1050-200 and Com-301LN) can be understood on the basis of the YS values of the DIM and austenite phases, and the low work-hardening of grain-refined austenite. As an example, we can predict the YS of the austenite phase (YS_{fcc}) in structures containing both DIM and austenite by using a simple summation Equation (2).

$$YS = x*YS_{bcc}+(1-x)*YS_{fcc} \Rightarrow YS_{fcc} = (YS_c - x*YS_{bcc})/(1-x) \quad (2)$$

where YS_{bcc} and YS_{fcc} are the YSs of martensite and austenite, respectively, and x is DIM fraction and $(1-x)$ is austenite fraction.

The YS of a fully martensitic structure with slight deformation can be assumed to be roughly 1100 MPa, as estimated from Fig. 24a, although higher values, 1200–1800 MPa, have been reported by various authors for cold-rolled martensite (e.g. Tomimura, Takaki & Tokunaga, 1991; Paper V). The YS_{fcc} in the 56CR-690-60 structure (Table 7) is then $(815-0.02*1100)/0.98 = 810$ MPa. After 20% rolling reduction, the YS of this structure was 960 MPa (Table 7) and the DIM fraction 38%, so the predicted YS_{fcc} is 874 MPa (assuming that no strengthening of DIM occurred). Thus, the amount of work-hardening of austenite by 20% CR reduction is from 810 to 874 MPa, i.e. only 8% in this FGA structure. Contrary to this, for the CGA structure, the very faint work-hardening of the reversed structures was also reflected in the tensile stress-strain curves as a long Lüders strain (Fig. 22), but we can now realise that the same phenomenon is present in CR, as well. In addition to the more efficient strain hardening of the CGA, the DIM has a stronger effect there due to the large relative strength difference between the CGA and DIM. This is seen in cyclic hardening under dynamic loading, as discussed in the next section.

5.3.3 Fatigue strength affected by microstructural features

It is well known that GS refinement improves static properties, e.g. (Kisko et al., 2011; Rajasekhara et al., 2007; Somani et al., 2009), as shown here, and also fatigue resistance, especially in the HCF regime (Di Schino & Kenny, 2013; Man et al., 2018). In the present study, the reversed structures with an AGS of 0.6–3.4 μm exhibited at least double fatigue strengths (stress amplitudes) compared with those of the coarse-grained ($\sim 20 \mu\text{m}$) reference structures. However, the highest fatigue strength was obtained with partially reversed structures containing retained phases among fine and ultrafine austenite grains. The effects of different microstructural features are discussed in the following.

The effect of GS on fatigue strength has been studied extensively also in austenitic stainless steels (Di Schino & Kenny, 2003; Droste et al., 2018; Fargas et al., 2015; Hamada & Karjalainen, 2010; Man et al., 2017, 2018; Poulon et al., 2010). Hamada & Karjalainen (2010) observed significant improvement in the fatigue life of reversion-treated 301LN steel in the 63CR-800-1 condition (AGS $\sim 0.5 \mu\text{m}$) under bending fatigue loading. Furthermore, crack nucleation tended to take place at grain boundaries, but not in slip bands or boundaries as it did in the CGA structure. Similar behaviour under axial fatigue was noticed in the present study. Droste et al. (2018) suggested that the small difference in hardness between austenite and DIM in the UFGA partially reversed structure would lead to more homogeneous strain distribution during cycling, whereas in the CGA structure strain is localised in the austenite phase. However, the behaviour of each phase of the reversed structures under cyclic loading, i.e. crack initiation and propagation stages, is outside the scope of this work and was only preliminarily investigated. As an example of the influence of the phases, crack nucleation along the grain boundaries of FSA grains while DA grains stay resistant is seen in Fig. 23.

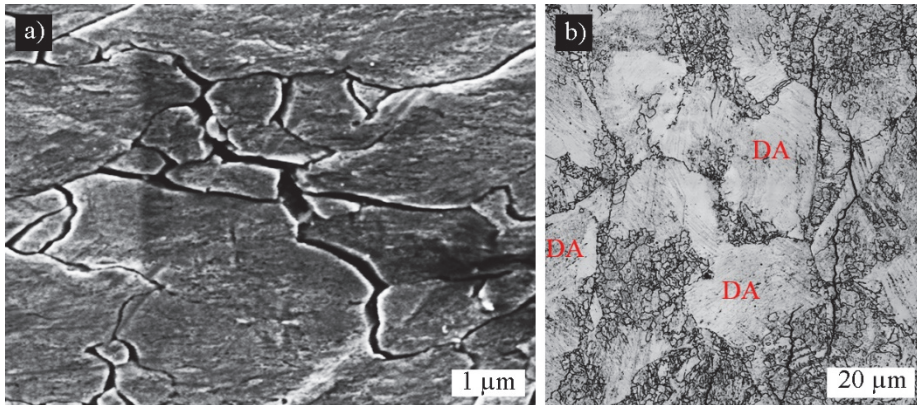


Fig. 23. Cracking (a) along the grain boundaries of submicron-sized austenite grains in the 63CR-800-1 structure and (b) in medium-sized austenite grains but outside of DA grains in the 32CR-750-0.1 structure. (Reprinted by permission from Paper II © 2014 Elsevier).

Hard martensite in the soft austenitic matrix is known to improve fatigue strength; e.g. (Biermann et al. 2016; Chlupova et al., 2014; Fargas et al., 2015; Glage, Weidner & Biermann, 2010; Glage, Weidner & Biermann, 2011; Hennessy et al., 1976; Mateo, Fargas & Zapata, 2012; Mateo, Zapata & Fargas, 2013; Topic et al., 2007). It has been systematically shown that an increase in the DIM fraction leads to higher fatigue strength in the HCF regime due to increased strength, but relatively, LCF strength is decreased due to impaired ductility. It has been argued that there is an upper limit to martensite fraction to improve fatigue resistance in the HCF regime, but the exact value seems to be unclear. For example, Topic et al. (2007) showed that in AISI 304-type steel (CGA condition), pre-formed DIM is beneficial for fatigue life if its fraction is below 20%. Mateo et al. (2012, 2013) found that even a 28% DIM fraction did not impair fatigue strength and Fargas et al. (2015) observed a clear improvement up to a 38% DIM fraction. The differences in the effect of DIM could be connected to GS, as suggested by Droste et al. (2018). Anyhow, as seen from Figs. 9d and 23b, the DIM fraction increases readily much beyond the 20–40% range, even up to 80% at the 0.6% strain amplitude, so that we may conclude that the low stability of low-temperature reversed structures is not beneficial in the LCF regime. At the 0.4% strain amplitude, the DIM fraction seems to stay below or around 20% (Fig. 9b). Thus, it can be expected that low stability

could enhance fatigue life at strain amplitudes of 0.4% or below (fatigue life more than 100 000 cycles).

As demonstrated in Section 4.4.3, the effect of rolling deformation on the fatigue strength of fine-grained structures remained marginal. This is because the initial strength difference between DIM and RA grains is small (1100 MPa vs. 850 MPa respectively) and fine-grained RA work-hardens only faintly in rolling deformation, as was shown in the previous section. Thus, fatigue strength must be based on a fine GS and low austenite stability. A fine GS and DIM formation increase the strength of the material, and due to the relatively low hardness difference between the phases, strain distribution is more homogenous during cycling, in contrast to coarser structures.

Martin, Wolf, Decker, Krüger & Martin (2015) and Weidner, Hangen & Biermann (2014) suggested that the main contribution to cyclic hardening is supplied by the reduced mean free path of dislocations. In the CGA structure, DIM formation occurs inside the deformation bands of austenite, but in the UFGA structure the DIM is nucleated at grain boundaries. It was expected that, in the UFGA structure, the DIM nuclei would grow rapidly into the entire grain, so the dislocation movement is blocked for only a few cycles, contrary to the CGA structure. Secondly, the grain size is refined in the CGA structure due to the small size of the DIM nuclei, but the difference is negligible in the UFGA structure.

The present experiments showed that the degree of cyclic hardening varied between the studied structures (Fig. 24a), even though the evolution of DIM was rather similar (Fig. 24b). This means that the effect of DIM transformation on cyclic hardening depends on the microstructure. To demonstrate this, we can do a few calculations. Similarly as in the previous section, the stress amplitude level of the fully martensitic structure is assumed to be 1100 MPa (Fig. 24). From Fig. 24a, it is seen that the initial stress amplitude of the CGA structure (63CR-1050-200) is about 350 MPa. Thus, we can predict that the stress amplitude at 1000 cycles due to DIM formation, when the DIM fraction is about 60% (Fig. 24b), is $0.4 \cdot 350 + 0.6 \cdot 1100 = 800$ MPa. Thus, the increase from 350 to 800 MPa is almost 130%. Correspondingly, for the partially reversed 63CR-750-0.1 structure (the initial stress amplitude is about 850 MPa), the stress amplitude after the formation of 60% DIM is $0.4 \cdot 850 + 0.6 \cdot 1100 = 940$ MPa, i.e. the increase from 850 to 940 MPa is only 11%. Hence, the same amount of DIM strengthens the soft CGA structure over 10 times more than the hard PRev structure.

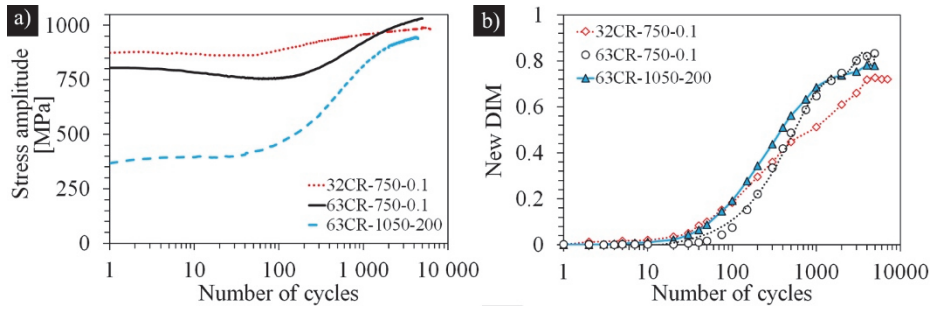


Fig. 24. Evolution of (a) stress amplitude and (b) DIM fraction during cycling at a strain amplitude of 0.6% for the 32CR-750-0.1, 63CR-750-0.1 and 63CR-1050 structures. (Modified from Paper III).

6 Future studies

The present work shows that low-temperature reversed structures consist of complex microstructural features affecting their behaviour and properties. The key for future research is not only to search for processing routes for enhancing the strength of commercial grades, but also to find possibilities for detailed scientific studies on novel microstructures. As an example, utilisation of a specially designed inductor with a separate rolling stand would allow multiple repetitions of reversion to conduct fundamental studies of highly refined structures. The technology has been tested during the follow-up research of this thesis for twice repeated reversion. The following topics could be studied:

- Development of a research environment for creating extremely fine-grained structures using repeated deformation and annealing steps by induction heating. Significantly refined grain sizes, but also larger sample sizes, would facilitate new research areas such as forming operations.
- Search for CR conditions that are most effective for DIM formation but also feasible for industrial practice.
- Search for optimal annealing routes (heating rate, T_p and t_s) for industrial manufacturing.
- Create and characterise highly refined structures with controlled a) homogenous and b) non-uniform grain distributions. Are coarser grains among nano-grains beneficial for strength and ductility?
- Study the effect of chemical banding existing on rolled sheets on reversion kinetics. Is it possible to utilise segregation to produce desired grain size distributions resulting from local stability differences?
- Create reversed structures with a yield strength over 1000 MPa using two approaches: 1) grain refinement by repeated reversion and 2) utilising highly deformed retained austenite (30–50%) to strengthen the reversed austenite structure. Both routes have already been successfully demonstrated in the follow-up research.
- Determine precipitation kinetics after different CR conditions; the effect of phase fractions and their deformation state on precipitation and consequently, austenite stability.
- Study the behaviour of the above-mentioned structures and their properties under monotonic and cyclic loading, their formability, machinability and corrosion resistance. Special interests should be addressed for studying

commercial advantages by taking into account the limitations of current temper-rolled austenitic steel grades, e.g. compression–tension anisotropy and fire resistance.

- The effect of welding on the microstructure and properties of reversed structures.
- Apply the newest knowledge on reversion treatment to practical applications such as pipe and tube manufacturing.

7 Summary and conclusions

The microstructures, behaviour and properties of reversion-treated austenitic stainless steel 301LN (18Cr-7Ni-0.16N) were investigated to better understand the microstructural features behind the enhanced properties of the fine-grained structures. Low prior cold rolling reduction of 32% was adopted in addition to 56% and 63%, the latter commonly used in earlier studies. Various microstructures were created using both a Gleeble simulator and a pilot induction (600 kW) heat treatment line. The created microstructures were characterised by employing various light and electron optical microscopes. Evolution of the martensite fraction during tensile and cyclic straining was measured magnetically using a Feritscope instrument. Fatigue tests were carried out under total strain-controlled loading. The main results and conclusions can be summarised as follows:

- Reversed structures are complex and non-uniform, consisting mainly of austenite with fine-sized (less than 3 μm) and medium-sized (3–10 μm) grains. The fraction of fine-sized grains increases as prior cold rolling reduction increases and/or the annealing temperature (at a given holding time) decreases.
- The medium-sized grains are formed mainly from slightly deformed martensite by both diffusional and shear reversion mechanisms.
- Partially reversed structures (created below 800 °C) also consist of varying fractions of strong retained phases, deformed austenite and martensite.
- The stability of reversed structures under dynamic and rolling straining seemed to vary similarly to stability under tensile straining.
- Austenite stability increases with decreasing grain size. However, some coarse austenite grains were stable due to their special orientation. In practice, medium-sized grains were most susceptible to martensite transformation. However, stability decreased significantly in spite of grain refinement during low-temperature reversion treatment at ≤ 850 °C as a result of nitride precipitation.
- The mechanical properties (tensile and fatigue) of the reversed structures were highly enhanced in comparison with those of a commercial grade. For example, the yield strength of the partially reversed structures was slightly higher and the fatigue strength was equal to that of the commercial grade after 20% strengthening rolling.
- The degree of cold rolling reduction did not affect the properties achieved, so that even reduction of 32% is applicable, although the average grain size

remains larger. The retained phases strengthen structures consisting of high fractions of medium-sized grains.

- Cyclic hardening of fine-grained reversed structures is faint compared with that of a coarse-grained structure, even though strain-induced martensite formation occurs to a similar extent. This is due to the small strength difference between fine grain-sized austenite and martensite.
- Subsequent cold rolling is not effective in enhancing mechanical properties. This is attributed to the small difference in the strength of fine-grained austenite and martensite, and the very low work-hardening of fine-grained austenite.

List of references

- Angel, T. (1954). Formation of martensite in austenitic stainless steels. *The Journal of the Iron and Steel Institute*, 177, 165–174.
- Baghbadorani, H. S., Kermanpur, A., Najafizadeh, A., Bejahti, P., Moallemi, M. & Rezaee, A. (2015). Influence on Nb-microalloying on the formation of nano/ultrafine-grained microstructure and mechanical properties during martensite reversion process in a 201type austenitic stainless steel. *Metallurgical and Materials Transactions A*, 46(8), 3406-3413. <https://doi.org/10.1007/s11661-015-2931-3>
- Beese, A. M. & Mohr, D. (2011). Identification of the direction-dependency of the martensitic transformation in stainless steel using in situ magnetic permeability measurements. *Experimental Mechanics*, 51, 667–676. <https://doi.org/10.1007/s11340-010-9374-y>
- Behjati, P., Kermanpur, A., Najafizadeh, A. & Samaei Baghbadorani, H. (2014). Effect of annealing temperature on nano/ultrafine grain of Ni-free austenitic stainless steel. *Materials Science and Engineering A*, 592, 77–82. <https://doi.org/10.1016/j.msea.2013.10.087>
- Biermann, H., Glage, A. & Droste, M. (2016). Influence of temperature on fatigue-induced martensitic phase transformation in a metastable CrMnNi-steel. *Metallurgical and Materials Transactions A*, 47(1), 84–94. <https://doi.org/10.1007/s11661-014-2723-1>
- Botshekan, M., Degallaix, S. & Desplanques, Y. (1997). Influence of martensitic transformation on the low-cycle behaviour of 316LN stainless steel at 77 K. *Materials Science and Engineering A*, 234–236, 463–466. [https://doi.org/10.1016/S0921-5093\(97\)00299-2](https://doi.org/10.1016/S0921-5093(97)00299-2)
- Böhner, A., Niendorf, T., Amberger, D., Höppel, H. W., Göken, M. & Maier, H. J. (2012). Martensitic transformation in ultrafine-grained stainless steel AISI 304L under monotonic and cyclic loading. *Metals* 2, 56–64, <https://doi.org/10.3390/met2010056>
- Calcagnotto, M., Adachi, Y., Ponge, D. & Raabe, D. (2011). Deformation and fracture mechanisms in fine- and ultrafine-grained ferrite/martensite dual-phase steels and the effect of aging. *Acta Materialia*, 59, 658–670. <https://doi.org/10.1016/j.actamat.2010.10.002>
- Challa, V. S. A., Misra, R. D. K., Somani, M. C. & Wang, Z. D. (2016). Strain hardening behavior of nanograined/ultrafine-grained (NG/UFG) austenitic 16Cr–10Ni stainless steel and its relationship to austenite stability and deformation behavior. *Materials Science and Engineering A*, 649, 153–157. <https://doi.org/10.1016/j.msea.2015.09.112>
- Charles, J., Mithieux J. D., Krauschick, J., Suutala, N., Antonio, S.J., Van Hecke, B. & Pauly, T. (2008). A new European 200 series standard to substitute 304 austenitics? In: *6th European Stainless Steel Conference, Science and Market*. Helsinki, Finland, 427-436. <https://doi.org/10.1051/metal/2009019>
- Chlupova, A., Man, J., Polák, J. & Karjalainen, L. P. (2014). LCF behaviour of ultrafine grained 301LN stainless steel. *Procedia Engineering*, 74, 147–150. <https://doi.org/10.1016/j.proeng.2014.06.239>

- Cooper, C. V. & Fine, M. E. (1984). Coffin-Manson relation for fatigue crack initiation. *Scripta Metallurgica*, 18(6), 593–596. [https://doi.org/10.1016/0036-9748\(84\)90347-8](https://doi.org/10.1016/0036-9748(84)90347-8)
- Cotterill, P. & Mould, P.R. Recrystallization and Grain Growth in Metals. London 1976. Surrey University Press. 409p.
- Das, A., Tarafder, S., Chakraborti, P. C. (2011). Estimation of deformation induced martensite in austenitic stainless steels. *Materials Science and Engineering A*, 529, 9–20. <https://doi.org/10.1016/j.msea.2011.08.039>
- De, A. K., Speer, J. G., Matlock, D. K., Murdock, D. C., Mataya, M. C. & Comstock Jr., R. J. (2006). Deformation- induced phase transformation and strain hardening in Type 304 austenitic stainless steel. *Metallurgical and Materials Transactions A*, 37A(6), 1875–1886. <https://doi.org/10.1007/s11661-006-0130-y>
- Di Schino, A., Barteri, M. & Kenny, J. M. (2002). Development of ultra fine grain structure by martensitic reversion in stainless steel. *Journal of Materials Science Letters*, 21, 751–753. <https://doi.org/10.1023/A:1015757710546.pdf>
- Di Schino, A. & Kenny, J. M. (2003). Grain size dependence of the fatigue behaviour of a ultrafine-grained AISI 304 stainless steel. *Materials Letter*, 57, 3182–3185. [https://doi.org/10.1016/S0167-577X\(03\)00021-1](https://doi.org/10.1016/S0167-577X(03)00021-1)
- Di Schino, A., Salvatori, I. & Kenny, J. M. (2002). Effects of martensite formation and austenite reversion on grain refining of AISI 304 stainless steel. *Journal of Materials Science*, 37, 4561–4565. <https://doi.org/10.1023/A:1020631912685>
- Dini, G., Najafizadeh, A., Ueji, R., Monir-Vaghefi, S. M. (2010). Improved tensile properties of partially recrystallized submicron grained TWIP steel. *Materials Letters*, 64, 15–18. <https://doi.org/10.1016/j.matlet.2009.09.057>
- Droste, M., Ullrich, C., Motylenko, M., Fleischer, M., Weidner, A.,... Biermann, H. (2018). Fatigue behavior of an ultrafine-grained metastable CrMnNi steel tested under total strain control. *International Journal of Fatigue*, 106, 143-152. <https://doi.org/10.1016/j.ijfatigue.2017.10.001>
- EN 1993-1-1 Eurocode 3: Design of Steel Structures (section 3.2.2)
- Eskandari Sabzi, H., Zarei Hanzaki, A., Abedi, H. R., Soltani, R., Mateo, A. & Roa, J. J. (2016). The effects of bimodal grain size distributions on the work hardening behaviour of a Transformation-Twinning induced plasticity steel. *Materials Science and Engineering A*, 678, 23–32. <https://doi.org/10.1016/j.msea.2016.09.085>
- Fargas, G., Zapata, A., Roa, J. J., Sapezanskaia, I. & Mateo, A. (2015). Correlation between microstructure and mechanical properties before and after reversion of metastable austenitic stainless steels. *Metallurgical and Materials Transactions A*, 46(12), 5697–5707. <https://doi.org/10.1007/s11661-015-3178-8>
- Forouzan, F., Najafizadeh, A., Kermanpur, A., Hedayati, A. & Surkialabad, R. (2010). Production of nano/submicron grained AISI 304L stainless steel through the martensite reversion process. *Materials Science and Engineering A*, 527(27-28), 7334-7339. <https://doi.org/10.1016/j.msea.2010.08.002>

- Glage, A., Weidner, A. & Biermann, H. (2010). Effect of austenite stability on the low cycle fatigue behavior and microstructure of high alloyed metastable austenitic cast TRIP steels. *Procedia Engineering*, 2(1), 2085–94. <https://doi.org/10.1016/j.proeng.2010.03.224>
- Glage, A., Weidner, A. & Biermann, H. (2011). Cyclic deformation behaviour of three austenitic cast CrMnNi TRIP/TWIP steels with various Ni content. *Steel Research International*, 82(9), 1040–7. <https://doi.org/10.1002/srin.201100080>
- Hahnenberger, F., Smaga, M. & Eifler, D. (2014). Microstructural investigation of the fatigue behavior and phase transformation in metastable austenitic steels at ambient and lower temperatures. *International Journal of Fatigue*, 69, 36–48. <https://doi.org/10.1016/j.ijfatigue.2012.07.004>
- Hamada, A. S. & Karjalainen, L. P. (2010). High-cycle fatigue behavior of ultrafine-grained austenitic stainless and TWIP steels. *Materials Science and Engineering A*, 527(21–22), 5715–5722. <https://doi.org/10.1016/j.msea.2010.05.035>
- Hamada, A. S., Karjalainen, L. P., Venkata Surya, P. K. C. & Misra, R. D. K. (2011). Fatigue behavior of ultrafine-grained and coarse-grained Cr-Ni austenitic stainless steels. *Materials Science and Engineering A*, 528, 3890–3896. <https://doi.org/10.1016/j.msea.2011.01.106>
- He, Y. M., Wang, Y. H., Guo, K. & Wang, T. S. (2017). Effect of carbide precipitation on strain-hardening behavior and deformation mechanism of metastable austenitic stainless steel after repetitive cold rolling and reversion annealing. *Materials Science and Engineering A*, 708, 248–253. <https://doi.org/10.1016/j.msea.2017.09.103>
- Hennessy, D., Steckel, G. & Altstetter, C. (1976). Phase transformation of stainless steel during fatigue. *Metallurgical and Materials Transactions A*, 7(3), 415–424. <https://doi.org/10.1007/BF02642838>
- Huang, J., Ye, X., Gu, J., Chen, X. & Xu, Z. (2012). Enhanced mechanical properties of type AISI301LN austenitic stainless steel through advanced thermo mechanical process. *Materials Science and Engineering A*, 532, 190–195. <https://doi.org/10.1016/j.msea.2011.10.080>
- Huang, J-X., Ye, X-N. & Xu, Z. (2012). Effect of cold rolling on microstructure and mechanical properties of AISI 301LN metastable austenitic stainless steels. *Journal of Iron and Steel Research*, 19(10), 59–63. [https://doi.org/10.1016/S1006-706X\(12\)60153-8](https://doi.org/10.1016/S1006-706X(12)60153-8)
- Iwamoto, T. & Tsuta, T. (2000). Computational simulation of the dependence of the austenitic grain size on the deformation behavior of TRIP steels. *International Journal of Plasticity*, 16, 791–804. [https://doi.org/10.1016/S0749-6419\(99\)00079-0](https://doi.org/10.1016/S0749-6419(99)00079-0)
- Jin, J. E., Jung, Y. S. & Lee, Y. K. (2007). Effect of grain size on the uniform ductility of a bulk ultrafine-grained alloy. *Materials Science and Engineering A*, 449–451, 786–789. <https://doi.org/10.1016/j.msea.2006.02.350>
- Jun, J. H. & Choi, C. S. (1998). Variation of stacking fault energy with austenite grain size and its effect on the Ms temperature of γ to martensitic transformation in Fe–Mn alloy. *Materials Science and Engineering A*, 257, 353–356. [https://doi.org/10.1016/S0921-5093\(98\)00994-0](https://doi.org/10.1016/S0921-5093(98)00994-0)

- Karjalainen L. P., Taulavuori, T., Sellman, M. & Kyröläinen, A. (2008). Some strengthening methods for austenitic stainless steels. *Steel research international*, 79(6), 404–412. <https://doi.org/10.1002/srin.200806146>
- Kisko, A., Hamada, A., Karjalainen, L. P. & Talonen, J. (2011). Microstructure and mechanical properties of reversion treated high Mn austenitic 204Cu and 201 stainless steels. In: *The 1st International Conference on High Manganese Steels (HMnS2011)*. Seoul, Korea, B-19.
- Kisko, A., Hamada, A. S., Talonen, J., Porter, D. & Karjalainen, L.P. (2016). Effects of reversion and recrystallization on microstructure and mechanical properties of Nb-alloyed low-Ni high-Mn austenitic stainless steels. *Materials Science and Engineering A*, 657, 359-370. <https://doi.org/10.1016/j.msea.2016.01.093>
- Kisko, A., Misra, R. D. K., Talonen, J. & Karjalainen, L. P. (2013). The influence of grain size on the strain-induced martensite formation in tensile straining of an austenitic 15Cr–9Mn–Ni–Cu stainless steel. *Materials Science and Engineering A*, 578, 408–416, <https://doi.org/10.1016/j.msea.2013.04.107>
- Krupp, U., West, C. & Christ, H-J. (2008). Deformation-induced martensite formation during cyclic deformation of metastable austenitic steel: influence of temperature and carbon content. *Materials Science and Engineering A*, 481–482, 713–717. <https://doi.org/10.1016/j.msea.2006.12.211>
- Leal, R. H. & Guimaraes, J. R. C. (1981). Microstructure evolution during mechanically induced martensitic transformation in Fe-31% Ni-0.1% C. *Materials Science and Engineering*, 48(2), 249–254. [https://doi.org/10.1016/0025-5416\(81\)90009-4](https://doi.org/10.1016/0025-5416(81)90009-4)
- Lee, Y. K. & Choi, C. S. (2000). Driving force for $\gamma \rightarrow \epsilon$ martensitic transformation and stacking fault energy of γ in Fe-Mn binary system. *Metallurgical and Materials Transactions A*, 31A, 355-360. <https://doi.org/10.1007/s11661-000-0271-3>
- Lee, S., Lee, S-J. & De Cooman, B. C. (2011). Work hardening behavior of ultrafine-grained Mn transformation-induced plasticity steel. *Acta Materialia*, 59(20), 7546–7553. <https://doi.org/10.1016/j.actamat.2011.08.030>
- Lee, T-H., Oh, C-S., Kim, S-J. (2008). Effects of nitrogen on deformation-induced martensitic transformation in metastable austenitic Fe–18Cr–10Mn–N steels. *Scripta Materialia*, 58, 110–113. <https://doi.org/10.1016/j.scriptamat.2007.09.029>
- Lee, S-J., Park, Y-M., Lee, Y-K. (2009). Reverse transformation mechanism of martensite to austenite in a metastable austenitic alloy. *Materials Science and Engineering A*, 515(1-2), 32-37. <https://doi.org/10.1016/j.msea.2009.02.010>
- Lee, T., Park, C. H., Lee, D-L. & Lee C. S. (2011). Enhancing tensile properties of ultrafine-grained medium-carbon steel utilizing fine carbides. *Materials Science and Engineering A*, 528, 6558–6564. <https://doi.org/10.1016/j.msea.2011.05.007>
- Lehto, P., Remes, H., Saukkonen, T., Hänninen, H. & Romanoff, J. 2014. Influence of grain size distribution on the Hall-Petch relationship of welded structural steel. *Materials Science and Engineering A*, 592, 28–39. <https://doi.org/10.1016/j.msea.2013.10.094>
- Lo, K. H., Shek, C. H. & Lai, J. K. L. (2009). Recent developments in stainless steels. *Materials Science and Engineering R*, 65, 39–104. <https://doi.org/10.1016/j.mser.2009.03.001>

- Machado, I. F., Carvalho, P. A. & Padilha, A. F. (2015). Austenite instability and precipitation behavior of high nitrogen stainless steels. In *Stainless Steel: Microstructure, Mechanical Properties and Methods of Application*; Pramanik, A., Kumar Basak, A., Eds.; Nova Science Publishers: New York, NY, USA, 1–36.
- Man, J., Chlupová, A., Kuběna, I., Kruml, T., Man, O.,... Polák, J. (2017). LCF behaviour of 301LN steel: coarse-grained vs. UFG-bimodal structure. In: *Proceedings of the LCF8 The Eighth International Conference on Low Cycle Fatigue*, Dresden, Germany, 27–29 June 2017.
- Man, J., Järvenpää, A., Jaskari, M., Kuběna, I., Fintová, S.,... Polák, J. (2018). Cyclic deformation behaviour and stability of grain-refined 301LN austenitic stainless structure. January 2018, MATEC Web of Conferences 165:06005, <https://doi.org/10.1016/j.mser.2009.03.001>.
- Maréchal, D. (2011). Linkage between mechanical properties and phase transformation in a 301LN austenitic stainless steel. Doctoral thesis, The University of British Columbia, Vancouver, p. 249. <https://doi.org/10.14288/1.0071814>
- Martin, S., Wolf, S., Decker, S., Krüger, L. & Martin, U. (2015). Deformation bands in high-alloy austenitic 16Cr6Mn6Ni TRIP steel: phase transformation and its consequences on strain hardening at room temperature. *Steel Research International*, 86(10), 1187–96. <https://doi.org/10.1002/srin.201500005>
- Martins, L. F. M., Plaut, R. L. & Padilha, A. F. (1998). Effect of carbon on the cold-worked state and annealing behaviour of two 18wt%Cr-8wt%Ni austenitic stainless steels. *The Iron and Steel Institute of Japan*, 38(6), 572–579. <https://doi.org/10.2355/isijinternational.38.572>
- Mateo, A., Fargas, G. & Zapata, A. (2012). Martensitic transformation during fatigue testing of an AISI 301LN stainless steel. *IOP Conference Series: Materials Science and Engineering*, 31, 012010. <https://doi.org/10.1088/1757-899X/31/1/012010>
- Mateo, A., Zapata, A. & Fargas, G. (2013). Improvement of mechanical properties on metastable stainless steels by reversion heat treatments. *IOP Conference Series: Materials Science and Engineering*, 48, 012001. <https://doi.org/10.1088/1757-899X/48/1/012001>
- Matsuoka, Y., Iwasaki, T., Nakada, N., Tsuchiyama, T. & Takaki, S. (2013). Effect of grain size on thermal and mechanical stability of austenite in metastable austenitic stainless steel. *The Iron and Steel Institute of Japan*, 3, 1224–1230. <https://doi.org/10.2355/isijinternational.53.1224>
- Misra, R. D. K., Challa, V. S. A., Venkatsurya, P. K. C., Shen, Y. F., Somani, M. C. & Karjalainen, L. P. (2015). Interplay between grain structure, deformation mechanisms and austenite stability in phase-reversion-induced nanograin/ultrafine-grained austenitic ferrous alloy. *Acta Materialia*, 84, 339–348. <https://doi.org/10.1016/j.actamat.2014.10.038>
- Misra, R. D. K., Nayak, S., Mali, S. A., Shah, J. S., Somani, M. C. & Karjalainen, L. P. (2009). Microstructure and deformation behavior of phase-reversion-induced nanograin/ultrafine-grained austenitic stainless steel. *Metallurgical and Materials Transactions A*, 40(10), 2498–2509. <https://doi.org/10.1007/s11661-009-9920-3>

- Misra, R. D. K., Nayak, S., Mali, S. A., Shah, J. S., Somani, M. C. & Karjalainen, L. P. (2010). On the significance of nature of strain-induced martensite on phase-reversion-induced nanograined/ultrafine-grained austenitic stainless steel. *Metallurgical and Materials Transactions A*, 41, 3–12. <https://doi.org/10.1007/s11661-009-0072-2>
- Misra, R. D. K., Nayak, S., Venkatasurya, P. K. C., Ramuni, V., Somani, M. C. & Karjalainen, L. P. (2010). Nanograined/ultrafine-grained structure and tensile deformation behavior of shear phase reversion-induced 301 austenitic stainless steel. *Metallurgical and Materials Transactions A*, 41, 2162–2174. <https://doi.org/10.1007/s11661-010-0230-6>
- Misra, R. D. K., Wan, X. L., Challa, V. S. A., Somani, M. C. & Murr, L. E. (2015). Relationship of grain size and deformation mechanism to the fracture behavior in high strength–high ductility nanostructured austenitic stainless steel. *Materials Science and Engineering A*, 626(25), 41–50. <https://doi.org/10.1016/j.msea.2014.12.052>
- Misra, R. D. K., Zhang, Z., Jia, Z., Somani, M. C. & Karjalainen, L. P. (2010). Probing deformation processes in near-defect free volume in high strength–high ductility nanograined/ultrafine-grained (NG/UFG) metastable austenitic stainless steels. *Scripta Materialia*, 63, 1057–1060. <https://doi.org/10.1016/j.scriptamat.2010.07.041>
- Misra, R. D. K., Zhang, Z., Jia, Z., Venkat Surya, P. K. C., Somani, M. C. & Karjalainen, L. P. (2011). Nanomechanical insights into the deformation behavior of austenitic alloys with different stacking fault energies and austenitic stability. *Materials Science and Engineering A*, 528, 6958–6963. <https://doi.org/10.1016/j.msea.2011.05.068>
- Misra, R. D. K., Zhang, Z., Venkatasurya, P. K. C., Somani, M. C. & Karjalainen, L. P. (2010). Martensite shear phase reversion-induced nanograined/ultrafine-grained Fe–16Cr–10Ni alloy. The effect of interstitial alloying elements and degree of austenite stability on phase reversion. *Materials Science and Engineering A*, 527, 7779–7792. <https://doi.org/10.1016/j.msea.2010.08.051>
- Muller-Bollenhagen, C., Zimmermann, M. & Christ, H.-J. (2010). Very high cycle fatigue behaviour of austenitic stainless steel and the effect of strain-induced martensite. *International Journal of Fatigue*, 32, 936–942. <https://doi.org/10.1016/j.ijfatigue.2009.05.007>
- Nohara, K., Ono, Y. & Ohashi, N. (1977). Composition and grain size dependencies of strain-induced martensitic transformation in metastable austenitic stainless steels. *The Iron and Steel Institute of Japan*, 63(5), 212–222. https://doi.org/10.2355/tetsutohagane1955.63.5_772
- Odnobokova, M., Belyakov, A. & Kaibyshev, R. (2015). Development of nanocrystalline 304L stainless steel by large strain cold working. *Metals* 5(2), 656–68. <https://doi.org/10.3390/met5020656>
- Padilha, A. F., Plaut, R. L. & Rios, P. R. (2003). Annealing of cold-worked austenitic stainless steels. *The Iron and Steel Institute of Japan*, 43, 135–143. <https://doi.org/10.1016/j.msir.2009.03.001>
- Pereloma, E., Gazder, A. & Timokhina, I. (2015). Retained austenite: transformation-induced plasticity. *Encyclopedia Iron Steel Alloys*, 3088–3103. <https://doi.org/10.1081/EEISA-120049200>

- Poulon, A., Brochet, S., Glez, J-C., Mithieux, J-D., Vogt, J-B. (2010). Influence of texture and grain size on martensitic transformations occurring during low-cycle fatigue of a fine-grained austenitic stainless steel. *Advanced Engineering Materials*, 12 (10), 1041–1046. <https://doi.org/10.1002/adem.201000079>
- Rajasekhara, S., Ferreira, P. J., Karjalainen, L. P. & Kyröläinen, A. (2007). Hall–Petch behavior in ultra-fine-grained AISI 301LN stainless steel. *Metallurgical and Materials Transactions A*, 38, 1202–1210. <https://doi.org/10.1007/s11661-007-9143-4>
- Rajasekhara, S., Karjalainen, L. P., Kyröläinen, A. & Ferreira, P. J. (2010). Microstructure evolution in nano/submicron grained AISI 301LN stainless steel. *Materials Science and Engineering A*, 527, 1986–1996. <https://doi.org/10.1016/j.msea.2009.11.037>
- Ravi Kumar, B. & Sharma, S. (2014). Recrystallization behavior of a heavily deformed austenitic stainless steel during iterative type annealing. *Metallurgical and Materials Transactions A*, 45, 6027–6038. <https://doi.org/10.1007/s11661-014-2543-3>
- Ravi Kumar, B., Sharma, S., Kashyap, BP. & Prabhu, N. (2015). Ultrafine grained microstructure tailoring in austenitic stainless steel for enhanced plasticity. *Materials & Design*, 68, 63–71. <https://doi.org/10.1016/j.matdes.2014.12.014>
- Rollett, A., Rohrer, G. S. & Humphreys, J. (2017). Recrystallization and Related Annealing Phenomena. Elsevier. 734p.
- Santacreu, P. O., Glez, J. C., Chinouilh, G. & Fröhlich, T. (2006). Behaviour model of austenitic stainless steels for automotive structural parts. *Steel Research International*, 77(9-10), 686–691. <https://doi.org/10.1002/srin.200606448>
- Shi, F., Wang, L. J., Cui, W. F. & Liu, C. M. (2008). Precipitation kinetics of Cr₂N in high nitrogen austenitic stainless steel. *The Journal of Iron and Steel Research, International*, 15, 72–77. [https://doi.org/10.1016/S1006-706X\(08\)60270-8](https://doi.org/10.1016/S1006-706X(08)60270-8)
- Shrinivas, V., Varma, S. K. & Murr, L. E. (1995). Deformation-induced martensitic characteristics in 304 and 316 stainless steels during room-temperature rolling. *Metallurgical and Materials Transactions A*, 26A(3), 661–671. <https://doi.org/10.1007/BF02663916>
- Simmons, J. W. (1996). Overview: High-nitrogen alloying of stainless steels. *Materials Science and Engineering A*, 207, 159–169. [https://doi.org/10.1016/0921-5093\(95\)09991-3](https://doi.org/10.1016/0921-5093(95)09991-3)
- Simmons, J. W., Covino, B. S., Hawk, J. A. & Dunning, J. S. (1996). Effect of nitride (Cr₂N) precipitation on the mechanical, corrosion, and wear properties of austenitic stainless steel. *The Iron and Steel Institute of Japan*, 36, 846–854. <https://doi.org/10.2355/isijinternational.36.846>
- Smaga, M., Walther, F. & Eifler, D. (2008). Deformation-induced martensitic transformation in metastable austenitic steels. *Materials Science and Engineering A*, 483–484, 394–397. <https://doi.org/10.1016/j.msea.2006.09.140>
- Somani, M. C., Juntunen, P., Karjalainen, L. P., Misra, R. D. K. & Kyröläinen, A. (2009). Enhanced mechanical properties through reversion in metastable austenitic stainless steels. *Metallurgical and Materials Transactions A*, 40(3), 729–744. <https://doi.org/10.1007/s11661-008-9723-y>

- Song, R., Ponge, D., Raabe, D., Speer, J. G & Matlock, D. K. (2006). Overview of processing, microstructure and mechanical properties of ultrafine grained bcc steels. *Materials Science and Engineering A*, 441, 1–17, <https://doi.org/10.1016/j.msea.2006.08.095>
- Takaki, S., Fukunaga, K., Syarif, J. & Tsuchiyama, T. (2004). Effect of grain refinement on thermal stability of metastable austenitic steel. *Materials Transactions*, 45, 2245–2251. <https://doi.org/10.2320/matertrans.45.2245>
- Takaki, S., Tomimura, K. & Ueda, S. (1994). Effect of pre-cold-working on diffusional reversion of deformation induced martensite in metastable austenitic stainless steel. *The Iron and Steel Institute of Japan*, 34, 522–527. <https://doi.org/10.2355/isijinternational.34.522>
- Talonen, J., Aspegren, P. & Hänninen, H. (2004). Comparison of different methods for measuring strain induced α' -martensite content in austenitic steels. *Materials Science and Technology*, 20, 1506–1512. <https://doi.org/10.1179/026708304X4367>
- Tamura, I. (1982). Deformation-induced martensitic transformation and transformation-induced plasticity in steels. *Metal Science*, 16, 245–253.
- Taulavuori, T., Aspegren, P., Säynäjäkangas, J., Salmén, J. & Karjalainen, P. (2004). The anisotropic behaviour of the nitrogen alloyed stainless steel grade 1.4318. In: *7th High nitrogen steels conference*. Ostend, Belgium, 405–411.
- Tomimura, K., Takaki, S., Tanimoto, S. & Tokunaga, Y. (1991). Optimal chemical composition in Fe-Cr-Ni alloys for ultra grain refining by reversion from deformation induced martensite. *The Iron and Steel Institute of Japan*, 31(7), 721-727. <https://doi.org/10.2355/isijinternational.31.721>
- Tomimura, K., Takaki, S. & Tokunaga, Y. (1991). Reversion mechanism from deformation induced martensite to austenite in metastable austenitic stainless steels. *The Iron and Steel Institute of Japan*, 31(12), 1431-1437. <https://doi.org/10.2355/isijinternational.31.1431>
- Topic, M., Tait, R. B. & Allens, C. (2007). The fatigue behaviour of metastable (AISI-304) austenitic stainless steel wires. *International Journal of Fatigue*, 29, 656–665, <https://doi.org/10.1016/j.ijfatigue.2006.07.007>
- Ueji, R., Tsuchida, N., Terada, D., Tsuji, N., Tanaka, Y., Takemura, A. & Kunishige, K. (2008). Tensile properties and twinning behavior of high manganese austenitic steel with fine-grained structure. *Scripta Materialia*, 59(9), 963-966. <https://doi.org/10.1016/j.scriptamat.2008.06.050>
- Varma, S. K., Kalyanam, J., Murr, L. E. & Srinivas, V. (1994). Effect of grain size on deformation-induced martensite formation in 304 and 316 stainless steels during room temperature tensile testing. *Journal of Materials Science Letters*, 13, 107–111. <https://doi.org/10.1007/BF00416816>
- Wang, Z. C. & Prangnell, P. B. (2002). Microstructure refinement and mechanical properties of severely deformed Al–Mg–Li alloys. *Materials Science and Engineering A*, 328, 87–97. [https://doi.org/10.1016/S0921-5093\(01\)01681-1](https://doi.org/10.1016/S0921-5093(01)01681-1)
- Wang, M-M., Tasan, C. C., Ponge, D., Kostka, A. & Raabe, D. (2014). Smaller is less stable: size effects on twinning vs. transformation of reverted austenite in TRIP-maraging steels. *Acta Materialia*, 79, 268–281. <https://doi.org/10.1016/j.actamat.2014.07.02>

Weidner, A., Hangen, UD. & Biermann, H. (2014). Nanoindentation measurements on deformation-induced α' -martensite in a metastable austenitic high-alloy CrMnNi steel. *Philosophical Magazine Letters*, 94(8), 522–30. <https://doi.org/10.1080/09500839.2014.941027>

Original publications

- I Järvenpää, A., Jaskari, M., Man, J. & Karjalainen, L. P. (2017). Austenite stability in reversion-treated structures of a 301LN steel under tensile loading. *Materials Characterization*, 127, 12–26. <https://doi.org/10.1016/j.matchar.2017.01.040>
- II Järvenpää, A., Jaskari, M. & Karjalainen, L. P. (2014). Effect of grain size on fatigue behaviour of Type 301LN stainless steel. *International Journal of Fatigue*, 65, 93–98. <https://doi.org/10.1016/j.ijfatigue.2013.05.012>
- III Järvenpää, A., Jaskari, M., Man, J. & Karjalainen, L. P. (2017). Stability of grain-refined reversed structures in a 301LN austenitic stainless steel under cyclic loading. *Materials Science & Engineering A*, 703, 280–292. <https://doi.org/10.1016/j.msea.2017.07.033>
- IV Järvenpää, A., Jaskari, M., Juuti, T. & Karjalainen, L. P. (2017). Demonstrating the effect of precipitation on the mechanical stability of fine-grained austenite in reversion-treated 301LN stainless steel. *Metals* 7, 344. <https://doi.org/10.3390/met7090344>
- V Järvenpää, A., Jaskari, M. & Karjalainen, L. P. (2018). Reversed microstructures and tensile properties after various cold rolling reductions in AISI 301LN Steel. *Metals* 8, 109. <https://doi.org/10.3390/met8020109>
- VI Järvenpää, A., Jaskari, M. & Karjalainen, L. P. (2018). Properties of induction reversion-refined microstructures of AISI 301LN under monotonic, cyclic and rolling deformation. *Materials Science Forum*, 941, 601–607. <https://doi.org/10.4028/www.scientific.net/MSF.941.601>

Reprinted with permission from Elsevier Ltd. (I–III), IMDB (IV, V) and Trans Tech Publications Ltd. (VI). Original publications are not included in the electronic version of the dissertation.

679. Paaso, Henna (2018) Direction of arrival estimation algorithms for leaky-wave antennas and antenna arrays
680. Pap, Nora (2018) Value-added processing of blackcurrants : use of membrane technologies for clarification and concentration of blackcurrant juice and extraction of anthocyanins from blackcurrant marc
681. Tolvanen, Jarkko (2018) Novel sensor and switch applications for flexible and stretchable electronic materials
682. Alatarvas, Tuomas (2018) Evolution of inclusion population in calcium treated ultra-high strength steels : novel applications of sample data treatment
683. Tomperi, Jani (2018) Predicting the treated wastewater quality utilizing optical monitoring of the activated sludge process
684. Fazel Modares, Nasim (2018) The role of climate and land use change in Lake Urmia desiccation
685. Kärnä, Aki (2018) Modelling of supersonic top lance and the heat-up stage of the CAS-OB process
686. Silvola, Risto (2018) One product data for integrated business processes
687. Hildebrandt, Nils Christoph (2018) Paper-based composites via the partial dissolution route with NaOH/urea
688. El Assal, Zouhair (2018) Synthesis and characterization of catalysts for the total oxidation of chlorinated volatile organic compounds
689. Akanegbu, Justice Orazulukwe (2018) Development of a precipitation index-based conceptual model to overcome sparse data barriers in runoff prediction in cold climate
690. Niva, Laura (2018) Self-optimizing control of oxy-combustion in circulating fluidized bed boilers
691. Alavesa, Paula (2018) Playful appropriations of hybrid space : combining virtual and physical environments in urban pervasive games
692. Sethi, Jatin (2018) Cellulose nanopapers with improved preparation time, mechanical properties, and water resistance
693. Sanguanpuak, Tachporn (2019) Radio resource sharing with edge caching for multi-operator in large cellular networks
694. Hintikka, Mikko (2019) Integrated CMOS receiver techniques for sub-ns based pulsed time-of-flight laser ranging

S E R I E S E D I T O R S

A
SCIENTIAE RERUM NATURALIUM
University Lecturer Tuomo Glumoff

B
HUMANIORA
University Lecturer Santeri Palviainen

C
TECHNICA
Senior research fellow Jari Juuti

D
MEDICA
Professor Olli Vuolteenaho

E
SCIENTIAE RERUM SOCIALIUM
University Lecturer Veli-Matti Ulvinen

E
SCRIPTA ACADEMICA
Planning Director Pertti Tikkanen

G
OECONOMICA
Professor Jari Juga

H
ARCHITECTONICA
University Lecturer Anu Soikkeli

EDITOR IN CHIEF
Professor Olli Vuolteenaho

PUBLICATIONS EDITOR
Publications Editor Kirsti Nurkkala

